

1 **Chemical characterization of freshly emitted**
2 **particulate matter from aircraft exhaust using**
3 **single particle mass spectrometry**

4
5 Manuel Abegglen¹, B. Brem², Martin Ellenrieder³, J. Wang², T. Rindlisbacher⁴, U.
6 Lohmann¹ and B. Sierau¹

7 1) Institute for Atmospheric and Climate Science, ETH Zurich, Switzerland

8 2) Laboratory for Advanced Analytical Technologies, EMPA, Dübendorf, Switzerland

9 3) SR Technics, Zurich, Switzerland

10 4) Swiss Federal Office of Civil Aviation, Bern, Switzerland

11
12 Corresponding author: Manuel Abegglen

13
14 Keywords: particulate matter aircraft engine exhaust, soot, single particle mass
15 spectrometry, metal tracers

16 Abstract

17 The chemical composition of non-volatile emission from aircraft engines was investigated
18 using single particle time-of-flight mass spectrometry. The exhaust from several engines was
19 sampled and analyzed. The soot particulate matter was sampled directly behind the
20 dismantled turbines running in a test cell at Zurich Airport. Single particle analyses focused
21 on the identification of the particle types with focus of metallic compounds. The particles
22 analyzed herein represent a subset of the emissions composing of the largest particles due to
23 instrumental restrictions. A vast majority of the analyzed particles were shown to contain
24 elemental carbon, and depending on the engine and the applied thrust the total carbon to
25 elemental carbon ratio ranged from 83 % to 99 %. The detected metallic compounds were
26 all internally mixed with the soot particles. The most abundant metals in the exhaust were
27 Cr, Fe, Mo, Na, Ca and Al; V, Ba, Co, Cu, Ni, Pb, Mg, Mn, Si, Ti and Zr were also detected.
28 We further investigated potential sources of the ATOFMS-detected metallic compounds
29 using Inductively Coupled Plasma Mass Spectrometry. The sources to be considered were
30 kerosene, engine lubricant oil and engine debris. An unambiguous source apportionment was
31 not possible because most metallic compound were detected in several of the analyzed
32 sources. Cobalt and zirconium were found to originate solely from engine wear. Non-volatile
33 aircraft engine emissions are an important anthropogenic source of soot particles in the upper
34 troposphere and in the vicinity of airports. They influence climate and contribute global
35 warming. In addition, they impact air quality and thus human health and the environment.
36 We provide fundamental information by presenting a chemical characterization of freshly
37 emitted particulate matter from aircraft engine exhaust useful for further research in these
38 fields.

39 1 Introduction

40 The continuous increase of commercial air traffic has led to rising public awareness and
41 concerns about the associated Particulate Matter (PM) emissions. The annual future growth
42 rate is estimated to be 3.4 % – 6.1 % (ICAO, 2013) in terms of passenger revenue kilometers.
43 Since it is much more complex and expensive to measure the mass and number based
44 emissions from aircraft engines than from other combustion sources (e.g. road traffic), the
45 legislation regarding aircraft emission are lagging behind general emission regulations. Up
46 to now, the standard way to regulate PM emissions for aircraft engines manufactured after
47 1983 is to limit smoke number (ICAO, 2008). Smoke number is a unit derived from filter
48 measurement using its change in reflectance after sampling a known volume of exhaust. In
49 the course of recent attempts to develop a new measurement standard for engine emission

50 certification, the Aviation Particulate Regulatory Instrumentation Demonstration
51 Experiment (A-PRIDE) campaigns were initiated. The A-PRIDE campaigns were conducted
52 at Zurich Airport in Switzerland. Previous studies from the A-PRIDE campaigns focused
53 primarily on the physical characterization of the exhaust particles (Durdina et al., 2014;
54 Abegglen et al., 2015) and evaluation of the entire system in order to demonstrate its
55 suitability for aircraft emissions (Lobo et al., 2015). Herein, we focus on the chemical
56 characterization of PM aircraft exhaust. The presented measurements were mainly
57 conducted during A-PRIDE 5 in 2013 investigating a CFM56-7B26/3 engine, using an
58 Aerosol Time-of-Flight Mass Spectrometer (ATOFMS, TSI Model 3800-030). The
59 ATOFMS allows to investigate the chemical composition of single particles, and the A-
60 PRIDE campaigns offered a great and rare opportunity to sample and study unaltered
61 combustion products from aircraft engines.

62 The emitted PM from aviation is of interest because it represents a unique anthropogenic
63 source of soot particles in the upper troposphere and in the vicinity of airports. These
64 particles alter the Earth's radiation budget in various ways depending on their physical and
65 chemical properties. Based on findings presented in the special report on aviation and the
66 global atmosphere (IPCC, 1999) and IPCC AR4 WG1 (IPCC, 2007), Lee et al. (2009)
67 divided the climate effects from aircraft PM on climate into three radiative forcing
68 components: soot aerosol, linear condensation trails (contrails), and induced cirrus
69 cloudiness, which are all believed to result in a warming. In addition, the emitted particles
70 could act as Ice Nucleating Particles (INP) and affect natural clouds.

71 Freshly emitted soot aerosol particles directly absorb and scatter solar radiation, primarily
72 due to their opaque appearance. The magnitude however depends (besides size and
73 morphology) on the chemical composition. A higher Elemental Carbon (EC) content for
74 example enhances absorption of radiation whereas a lower EC content leads to an increase
75 of the single scattering albedo (Qiu et al., 2014). Linear contrails form just behind aircraft
76 due the emission of heat and water vapor and formation depends on the ambient temperature
77 and humidity as well on the exhaust temperature and mixing processes after emission. The
78 cooling of the exhaust stream causes the water vapor to condense onto a fraction of the
79 emitted particles and to freeze subsequently if the temperature is sufficiently low. Contrails
80 result in a positive radiative forcing due to their occurrence in high altitudes. Similarly to
81 thin cirrus clouds, they reflect little incoming solar radiation back to space absorb terrestrial
82 infrared radiation. Their global coverage for the year 2006 was detected via satellite to be
83 0.07 % (Duda et al., 2013). Research on occurrence and formation of contrails dates back
84 almost 100 years and is well summarized in the review article from Schumann (1996). If the
85 ambient air is supersaturated with respect to ice, the formed ice particles continue to grow
86 and can form a persistent contrail. The largest radiative forcing arises from the induced cirrus
87 cursed by the possible evolution of linear contrails into persisting cirrus clouds (Burkhardt
88 & Kärcher, 2011). These spreading cirrus clouds can also become undistinguishable from
89 naturally (e.g. synoptically or orographically) evolved cirrus clouds. With a confidence of
90 90 %, the aviation-induced radiative forcing in 2005 was estimated to be in the range of 23
91 $\text{mW/m}^2 - 87 \text{mW/m}^2$ without aviation-induced cirrus and $38 \text{mW/m}^2 - 139 \text{mW/m}^2$ including

92 cirrus cloud formation, corresponding to a contribution to the anthropogenic forcing of 4.9
93 % (2 % – 14 %) (Lee et al., 2009).

94 Moreover, it has been found that some fraction of carbon-containing particles are efficient
95 Ice Nucleating Particles (INP) (Cozic et al., 2008). Thus, aircraft emissions can lead to
96 regionally increased INP concentration affecting natural cirrus clouds even in the absence of
97 contrail formation (Kärcher et al., 2007), including changes in optical properties, delays of
98 onsets and replacements (Burkhardt & Kärcher, 2011). This is explained by additional
99 heterogeneous INP inhibiting the homogeneous freezing of the background aerosol particles,
100 due to the decreased water content available. The magnitude of this effect remains uncertain
101 because it depends heavily on the ice-nucleating efficiency of the emitted soot particles and
102 of the background aerosol particles which are not yet completely understood (Zhou &
103 Penner, 2014). A study performed by Cziczo et al. (2013) tackling the properties of INP in
104 the upper troposphere showed that a dominant fraction of Ice Residuals (IR) collected in
105 cirrus clouds contain metal compounds such as sodium, potassium, copper, lead and iron.
106 These compounds have also been found in aircraft emissions by sampling the exhaust
107 (Agrawal et al., 2008). Also, Cziczo et al. (2009) showed that lead-containing are efficient
108 INP, as a consequence, lead- or metal-containing particles might increase the INP number
109 in the atmosphere. Thus, a thorough chemical characterization of single particles from fresh
110 aircraft PM emissions provides information to study the link between aircraft emissions and
111 ice formation processes in the atmosphere.

112 The radiative and ice-nucleating properties change over time as the soot particles undergo
113 aging by the uptake of water and/or secondary volatile species and oxidation. These
114 processes are partly influenced by the particle's initial composition (Rudich et al., 2007).
115 The Organic Carbon (OC) components on the particle surface were found to be important
116 for the aging process of soot and may even alter the Cloud Condensation Nuclei (CCN) or
117 IN activity when they oxidize by O₂ under solar radiation and turn into soluble organics (Han
118 et al., 2012). The initial chemical composition of the single particles is therefore of
119 importance because it influences their aging process and also changes in their ability to act
120 as CCN and INP.

121 Aviation PM emissions are also of importance as PM in general is known to cause adverse
122 health issues. The emitted particles have been shown to be small with a geometric mean
123 diameter well below 100 nm (Abegglen et al., 2015) and therefore fall mainly into the
124 particle class described as ultrafine PM (PM_{0.1}). Ultrafine particles can penetrate deeper into
125 the human respiratory system and are less likely to be removed than larger particles and may
126 be able to enter the blood stream (Terzano et al., 2010). Health effects in general seem to be
127 more associated with Black Carbon emission (BC) than with PM₁₀ or PM_{2.5} alone (Janssen
128 et al., 2012), but it was not possible to show that EC directly is a toxic component. Janssen
129 et al. (2012) therefore summarizes that BC probably acts as a carrier for toxic substances.
130 This supports findings from an earlier study showing that particles containing metals such
131 as vanadium, iron, copper and nickel can cause epithelial injuries (Pagan et al., 2003). It
132 seems intuitive that the largest respiratory health effects caused by aircraft emissions are
133 found in the vicinity of airports, especially for workers at airports (Touri et al., 2013).

134 However, emissions can cause health effects not only in the vicinity of airports but also on
135 larger spatial scales (Yim et al., 2015).

136 Earlier studies on PM aircraft emissions focused primarily on the particle size and
137 concentration in proportion to the thrust applied to the engine (Petzold & Schröder, 1998;
138 Rogers et al., 2005; Corporan et al., 2008; Herndon et al., 2008; Onasch et al., 2009).
139 Investigations on the composition in terms of organic content have also been performed
140 (Onasch et al., 2009; Timko et al., 2010; Lobo et al., 2015). Kinsey et al. (2011) sampled
141 exhaust plume from commercial aircraft at a distance of ~30 m behind the engine using
142 optical instruments to provide data on BC concentrations and gravimetric analysis of filters
143 to investigate the elemental composition quantitatively. However, the investigation of
144 aircraft PM emission in terms of chemical characterization from single particles is still in an
145 early stage and few studies exist. Demirdjian et al. (2007) sampled soot particles emitted by
146 an aircraft gas turbine engine directly behind the engine duct in order to investigate the
147 composition of soot agglomerates. The sample was then deposited on copper microgrids and
148 analyzed. They have found impurities of Fe, O, S, K and Mn. Mazaheri et al. (2013) collected
149 PM₁ samples on filters and membrane grids 200 m from an airfield runway in order to
150 perform elemental analysis on discrete particles using energy dispersive X-ray spectroscopy.
151 They found C, O, S, Cl, Na, Al, Si, Ca, Ti, Cr, Fe, Co, Ni, Cu, Zn, and Pb but attributed them
152 not only to engine exhaust but to a diverse range of sources such as tire wear, dust and traffic.
153 Especially studies on fresh aircraft exhaust sampled directly behind the engine remain scarce
154 and no study exists to our knowledge that investigates the chemical composition of freshly
155 emitted aircraft exhaust particles using in-situ single particle mass spectrometry. Our study
156 focuses on a general chemical characterization of single particles sampled directly behind
157 the engine with emphasis on metallic compounds in the particles.

158 2 Methods

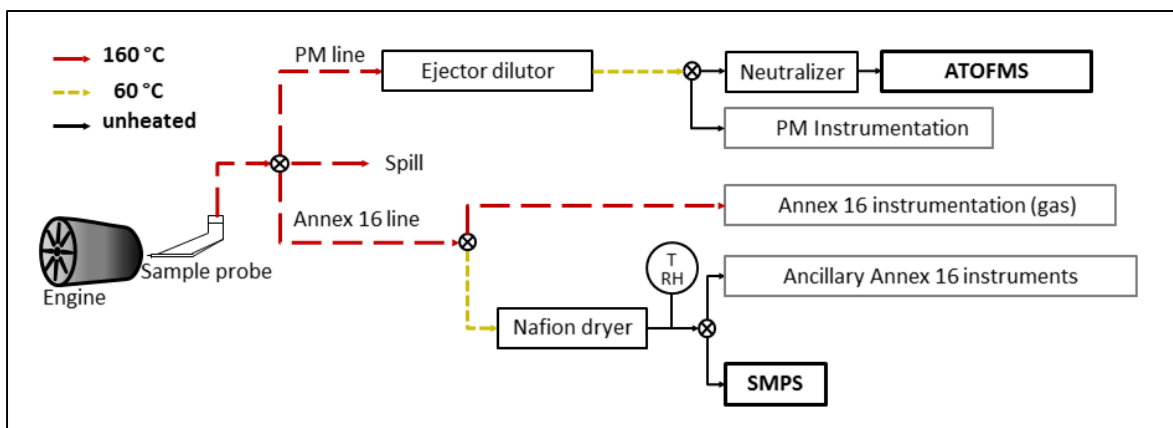
159 2.1 Measurement Campaigns and Location

160 The majority of the measurements presented herein were conducted during the dedicated
161 Aviation - Particle Regulatory Instrument Demonstration Experiment 5 (A-PRIDE 5)
162 campaign conducted in July and August 2013. Additional data was collected during A-
163 PRIDE 7 conducted in October 2014 and during piggyback measurements in June 2013 and
164 in Mai 2015. The campaigns took place at the airport Zurich where the measured were
165 conducted in a test cell. The facility is located in the southeastern corner of the airport area.
166 A tram route and a road are going by in the east of the test cell at a distance of <50 m and a
167 freeway at ~100 m. The engine under investigation during A-PRIDE 5 was a CFM56-
168 7B26/3, widely used in commercial aircraft including Boeing aircraft. This engine has a
169 single annular combustor and a maximum rated thrust of 117 kN. Two additional engine

170 types were investigated during piggyback tests, namely a CFM56-5B4/P and a CFM56-5C4.
 171 The CFM56 series are high-bypass turbofan engines. The CFM56-5B4/P engine has a dual
 172 annular combustor for reduced NO_x emission, whereas the CFM56-5C4 engine has a single
 173 annular combustor, having a maximum rated thrust of 120 kN and 151 kN, respectively. The
 174 CFM56-7B26/3 and the CFM56-5B4/P engine are both core flow engines where is the
 175 exhaust does not get mixed with bypass air from the ambient before leaving the engine duct,
 176 whereas the CFM56-5C4 is a mixed flow engine whose exhaust is diluted with bypass air at
 177 a ratio of ~1:6. All engines were fueled with commonly used Jet A-1 kerosene.

178 2.2 Experimental Set-up

179 The emitted particles were sampled by a probe oriented parallel to the exhaust flow (Figure
 180 1). The sampling probe was positioned at a distance of ~0.7 m behind the engine duct,
 181 guiding the emissions through an 8 mm inner diameter stainless steel pipe to the sampling
 182 system. A tee was used to split the sample into two main measurement lines referred to as
 183 the PM line and the Annex 16 line. The line was mainly used for measurements of non-
 184 volatile PM number and mass whereas the Annex 16 line was mainly used to measure
 185 gaseous species. Both lines were conductive PTFE and ~25 m in length before leading to the
 186 measuring instruments. Both lines were heated in order to prevent condensation of volatile
 187 species onto the sampled particles. The PM line was diluted by a factor of ~8–12 with
 188 synthetic air (grade 5.0) using a Dekati ejector dilutor (Dekati, Model DI 1000, Dekati Ltd.,
 189 Kangasala, Finland). This line was heated to 160 °C for the first ~7 m upstream of the ejector
 190 dilutor and then to 60 °C. This line was used for the PM instrumentation and the ATOFMS.
 191 The Annex 16 line was also heated to 160 °C leading to the Annex 16 instrumentation. A
 192 tee in this line was used to guide the sample through a 60 °C heated line through a Nafion
 193 (Perma Pure, Model PD-100T-24 (MSS), Perma Pure LLC, Toms River, USA) dryer to the
 194 ancillary Annex 16 instruments and a Scanning Mobility Particle Sizer (SMPS, TSI, Model
 195 3936, TSI Inc., St. Paul, USA) system. See Lobo et al. (2015) for a more detailed overview
 196 of the additional instruments and first results from this experimental set-up.



197
 198 Figure 1 Simplified schematic of the experimental set-up used.

199 2.3 Instruments

200 2.3.1 Aerosol Time-of-Flight Mass Spectrometer

201 An Aerosol Time-of-Flight Mass Spectrometer (ATOFMS, TSI Model 3800-030) was used
202 to investigate the single particle chemical composition of non-volatile fresh emissions from
203 aircraft engines. The ATOFMS is a mass spectrometer that measures the chemical
204 composition of single particles and their vacuum aerodynamic diameter (d_{ae}) (Gard et al.,
205 1997) and has the capability to resolve refractory material such as EC as well as metallic
206 compounds. Each mass spectra obtained allows the chemical analysis of this particle.

207 The ATOFMS works at low pressures which draws the sample flow into the instrument. It
208 consists of three main regions with decreasing working pressures: 1) the particle sampling
209 region (~ 270 Pa), 2) the particle sizing region ($\sim 10^{-3}$ Pa), and 3) the mass spectrometry
210 region ($\sim 10^{-6}$ Pa). The sample flow rate into the instrument was 0.1 l/min, set by a critical
211 orifice. A backup flow between 1 l/min and 3 l/min (depending on the flow needed by other
212 instruments) was used to shorten the response time. Downstream of the critical orifice, the
213 particles pass through an Aerodynamic Focusing Lens (AFL) that aligns the particles into a
214 narrow beam and then into the sampling region. For this study, an AFL optimized for an
215 aerodynamic particle size range from 30 nm to 300 nm was used (TSI, 2004). Once the
216 particles are in the sizing region, they accelerate due to the pressure drop depending on their
217 size and are detected by two consecutive continuous, orthogonally oriented wave diode-
218 pumped lasers ($\lambda = 532$ nm). The time they need to travel between the sizing lasers is used
219 to determine their aerodynamic size and to trigger the ionization laser in the following. The
220 particles then enter the mass spectrometry region where the particles are ionized by the
221 ionization laser (Nd:YAG, $\lambda = 266$ nm), set to an energy of ~ 1 mJ/pulse. If the particle is hit
222 by the ionization laser, it gets ablated and ionized, resulting in ions and molecules, both
223 positive and negative. They are then separated according to their mass-to-charge ratio (m/z)
224 by their mass-dependent acceleration in positive and negative electromagnetic fields in the
225 flight tubes. The time (of flight) the individual constituents need to travel through the
226 electromagnetic fields until they reach detector plates is recorded and converted into m/z
227 values. The output is a positive and negative mass spectra for each ionized particle, revealing
228 its aerodynamic size and chemical composition.

229 Before the particles entered the ATOFMS they were treated with a 210^{P0} neutralizer in order
230 to minimize their electric charge increasing the hit rate (fraction of sized/registered particles
231 that are ionized). This is because electrostatic forces can cause deviation of the particle's
232 trajectory within the instrument.

233 The ATOFMS data itself is not quantitative because of several reasons. For example, the
234 coating of a particle with secondary species were shown to decrease the ionization efficiency
235 resulting in changes in the measured ion peak areas (Hatch et al., 2014). Moreover, different
236 chemical species in the same particle can influence each other's ionization efficiencies due
237 to the so-called matrix effects (Liu et al., 2000). Nevertheless, analysis of spectra from the
238 same particle type using relative peak areas can reduce matrix effects to a certain extent
239 because of lower spectrum to spectrum variability (Gross et al., 2000). Thus, average relative

240 intensities from a large number of similar particles can be used to gain some information on
241 relative differences in the mass of compounds in the particle when comparing different
242 conditions.

243 2.3.2 Inductively Coupled Plasma Mass Spectrometry

244 Inductively Coupled Plasma Mass Spectrometry (ICP-MS) is an offline method often used
245 to measure metals from a bulk sample. It is very sensitive to the concentration of the analyzed
246 compounds which can be as low as one part in 10^{-15} . It uses argon treated with a high
247 frequency current in order to heat it up to 10 000 K, turning the argon into a plasma. The
248 sample is introduced with argon as carrier gas into the argon plasma where it is vaporized,
249 atomized and ionized. (J. H. Gross, 2011). The resulting ions are accelerated by an
250 electromagnetic field and subsequently registered by detectors, and quantification is
251 achieved by comparison with certified reference materials.

252 2.4 Data Analysis

253 2.4.1 Identification of particle types and components

254 The mass spectra were analyzed using MS-Analyze and ENCHILADA (Environmental
255 Chemistry through Intelligent Atmospheric Data Analysis) (Gross et al., 2010), two software
256 programs designed to analyze ATOFMS data. This allowed further size resolved analysis of
257 the particles or subclasses of particles using queries. Queries allow the identification of the
258 compounds of particles by searching for the corresponding m/z values.

259 ENCHILADA was used for a cluster analysis of the analyzed particles. It groups similar
260 spectra into clusters using different clustering algorithms (Giorio et al., 2012). Each resulting
261 cluster is representative for a particle types that show specific m/z values and ratios of
262 intensities. This study used k-means because only a small number of clusters were expected
263 due to the high resemblance of the spectra. Similar clusters were manually merged together.
264 The data presented in this study were analyzed with respect to engine thrust if enough data
265 was obtained, i.e. the A-PRIDE 5 measurements. The particles were characterized with
266 emphasis on the occurrence of metallic compounds. If interference with other peaks from
267 other ions was observed, peaks from isotopes of the metallic compounds were used to
268 discriminate.

269 Ratios of Elemental to Total Carbon (EC/TC) ratio were derived from ATOFMS data
270 adopting a method using the sum of relative peak areas associated with EC and TC presented
271 by Ferge et al. (2006). TC is defined as the sum of Organic Carbon and EC. After subtracting
272 peaks from known inorganic compounds from the average spectrum, TC was calculated by
273 adding up all remaining peak areas. The list of inorganic compounds from Ferge et al. (2006)
274 was modified by adding the metallic compounds found during our analysis. EC was
275 calculated from the average spectrum by adding up all peak areas at m/z $12i$, $12i + 1$, $12i +$
276 2 and $12i + 3$ (with $i = 1, 2$, etc.). The ratio of the obtained peak areas for EC and TC then
277 yielded the presented EC/TC values. This method was found to agree with a standardized
278 thermo-optical approach using the NIOSH 5040 method and a thermo-coulometric methods,

279 especially for samples with low inorganic content. Additionally, the particles were classified
280 into ‘EC’ and ‘ECOC’ using criteria such that the ‘EC’ class composed particles with no OC
281 whereas the ‘ECOC’ class composed particles showing both EC and OC. This was done by
282 applying an “exclusive” classification query on the obtained positive spectra in MS-Analyze.
283 This means, if particles are sorted into the first class for which they meet the prescribed
284 requirements, they are then excluded from further classification. The first class comprised
285 the ‘EC’ particles. In order to define the ‘ECOC’ class, two additional classes, ‘EC + K’ and
286 ‘K noEC noOC’, had to be defined and classified in advance because of the ambiguous
287 association of the $m/z+39$ peak with organic compound and potassium. This excludes the
288 possibility of having particles in the ‘ECOC’ class that contain EC and potassium and no
289 OC. The first additional class labelled as ‘EC + K’ was defined to show a peak at $m/z+39$
290 and the EC peaks. The second one labelled as ‘K noEC noOC’ was defined to show solely
291 $m/z+39$ while not showing the other peaks associated with OC. Note that the presence of
292 EC in the ‘K noEC noOC’ class is excluded due to the previous classification. Eventually,
293 the ‘ECOC’ class was defined to consist of the remaining particles showing any combination
294 of the OC and EC markers.

295 2.4.2 Particle size analysis

296 The vacuum aerodynamic diameter (d_{va}) of the aircraft soot particles was measured by the
297 ATOFMS. d_{va} was converted into electrical mobility diameter (d_m) in order to compare d_{va}
298 to continuous size measurements performed by a Scanning Mobility Particle Sizer (SMPS,
299 TSI, Model 3936, TSI Inc., St. Paul, USA) system, which measures d_m . The calculation was
300 done using equation [50] in DeCarlo et al. (2004):

$$301 \quad d_{va} = \frac{\rho_p d_m}{\rho_0 \chi_v^{3/2}}$$

302 ρ_p and ρ_0 are the particle density and unit density respectively and χ_v is the dynamic shape
303 factor in the vacuum or free molecular regime. ρ_p was assumed to be equal to the particle
304 material density of soot. This holds for aggregates with no internal voids such as freshly
305 evolved unaltered soot particles, and is supported by TEM pictures from aircraft soot (Liati
306 et al., 2014; Boies et al., 2015). A value for ρ_p of 1.87 g/cm^3 as estimated from our previous
307 effective density measurement on aircraft exhaust (Abegglen et al., 2015) was assumed.
308 Other reported values of ρ_p range from $1.7 \text{ g/cm}^3 \pm 0.7 \text{ g/cm}^3$ for non-volatile components
309 of diesel soot Park et al. (2004) up to 2.03 g/cm^3 (Braun et al., 2004) also for diesel soot. χ_v
310 was calculated using equations [2.1] and [2.2] as described in Shapiro et al. (2012) with the
311 information on particle mass and d_m also measured during A-PRIDE 5. Because the mass at
312 a certain size additionally depends on the engine’s thrust setting the mass was averaged. The
313 value of χ_v is size-dependent and was calculated using a power law fit taking into account
314 values obtained at different d_m .

315 3 Results and Discussion

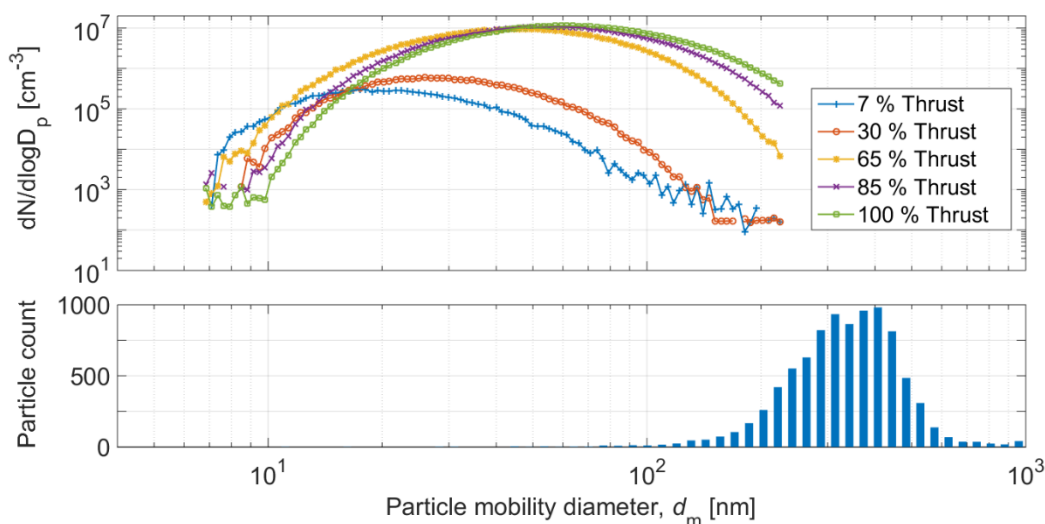
316 This chapter first gives an overview on the size of the investigated particles from aircraft
317 engine exhaust. Information on the chemical composition of the identified particle types is
318 provided, followed by Elemental Carbon (EC) to Total Carbon (TC) ratios determined from
319 ATOFMS data. Lastly, the occurrence of metal compounds detected in the particles are
320 presented and potential sources thereof are discussed. The latter is supported by ICP-MS
321 analyses of the most likely sources that are engine jet fuel, lubricant oil and engine wear.

322 During the A-PRIDE 5 campaign, the ATOFMS was not able to record both the positive and
323 the negative ion spectra because of instrumental restrictions. Thus, the vast majority of the
324 data consists of positive spectra. It was possible to measure negative spectra during the last
325 two days of the campaign, by switching the polarities of the high voltages applied to the
326 flight tubes of the ATOFMS.

327 3.1 Size of investigated particles

328 The upper panel of Figure 2 depicts the averaged thrust dependent SMPS measured size
329 distributions shown in represent of the mobility diameter emitted by the CFM56-7B26/3
330 engine collected via both, the PM line and the Annex 16 line. The lower panel shows the
331 mobility diameter, calculated from the measured aerodynamic size as explained in 2.4.2 of
332 the hit (i.e. chemically analyzed) particles by the ATOFMS during A-PRIDE 5.

333
334



335

336 Figure 2 Size distributions measured by SMPS on the sampling line (top) and the calculated size of the
337 chemically analyzed particles by the ATOFMS (bottom).

338 The mode of the SMPS size distribution lies between 20 nm and 50 nm. By extrapolating
339 the data, the measured mobility size ranges from <10 nm to ~600 nm. The size distribution
340 of particles that were hit by the ATOFMS, however, shows a mode at ~400 nm and ranges
341 from ~100 nm to ~700 nm. The exact mobility size distribution of the hit particles remains
342 unknown because the material density was assumed, and if it was higher, then the values
343 calculated for d_m would be lower. Nevertheless, the size distributions would still differ in
344 their modes, and the results show that the ATOFMS primarily sampled and analyzed the
345 largest particles emitted by the aircraft engines. The reason for the surprisingly large
346 difference in the particle size distribution remains unclear. Although, within the investigated
347 size-range differences in the chemical composition of the investigated particles were not
348 observed, our results cannot be reliably extrapolated towards smaller particles. Thus, the
349 results presented in the following are only representative for the largest particles in the
350 exhaust.

351 Experimental studies on the ice nucleating ability of soot showed that larger particles
352 generally are more efficient IN than smaller ones (Paul J. DeMott, 1990; Diehl & Mitra,
353 1998). Thus, assuming that particles emitted by aircraft engines are IN active, their
354 efficiency to act as IN probably also increases with increasing particle size. Because we
355 sampled the largest particles with the ATOFMS, they can be considered the fraction that is
356 likely to be the most important regarding the contribution of aircraft emissions to INP.

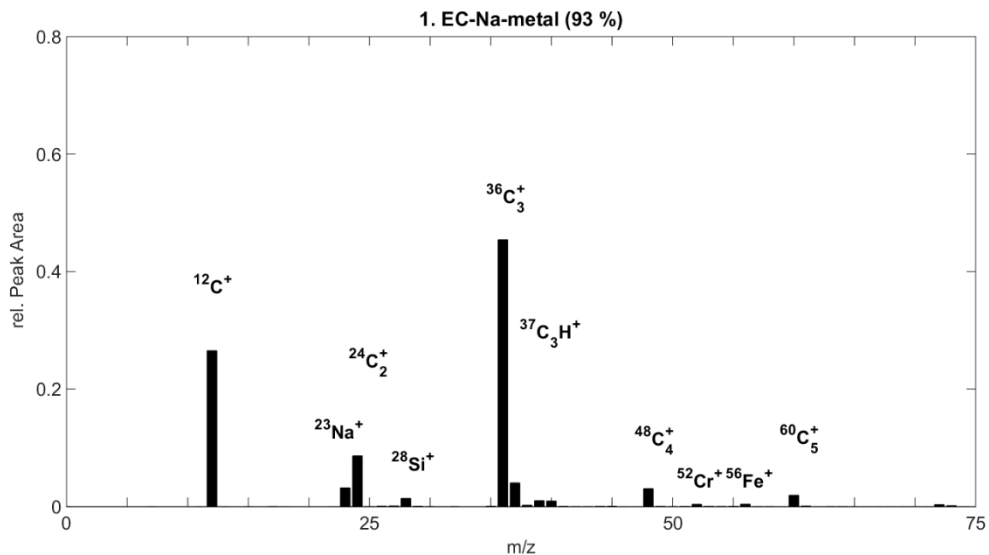
357 3.2 Chemical characterization

358 3.2.1 CFM56-7B26/3 engine

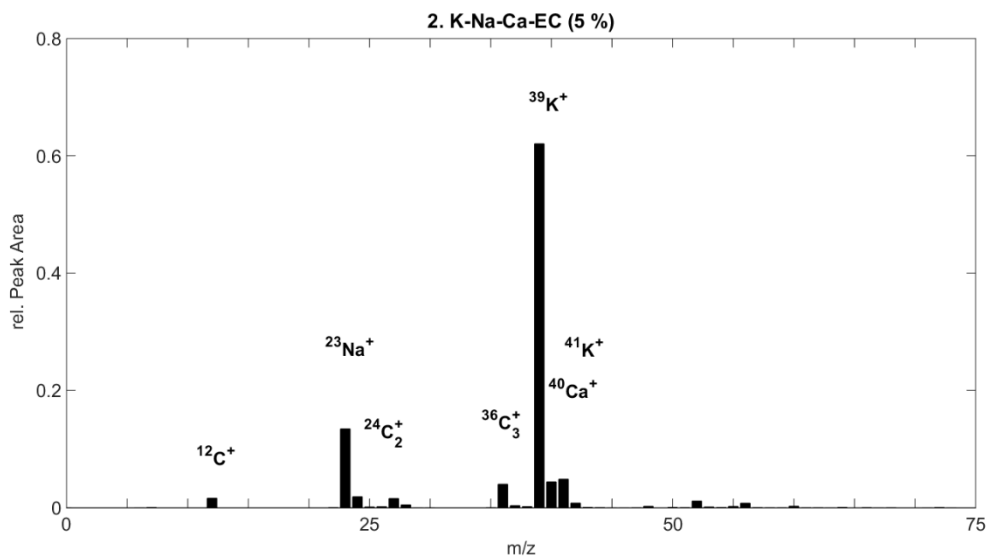
359 For the spectra recorded during A-PRIDE 5 the clustering and the subsequent interpretation
360 of the particle types were affected by the lack of negative mass spectra. In total 9875 positive
361 spectra were obtained. The analysis of the mass spectra obtained from particles emitted by
362 the CFM56-7B26/3 engine yielded six clusters.

363 The mass spectra of the three major clusters (Figure 3) represent >99 % of the particles, the
364 most prominent of which comprised ~93 % of all chemically analyzed particles. They were
365 classified as: (1) **EC-Na-metal** particles with a strong EC signature (m/z +12, +24, +36, +48,
366 +60, +72, +84) and small peaks of inorganic compounds from sodium (m/z +23) and metals
367 such as chromium (m/z +52) and iron (m/z +56). A small hydrocarbon peak (m/z +37 (C₃H))
368 indicates the presence of organic carbon (Spencer & Prather, 2006). The **K-Na-Ca-EC**
369 particle type (2) has a dominant potassium signal (m/z +39, +41) and a sodium peak while
370 including the EC pattern. This cluster comprises ~5 % of the particles. The **Ca-Al-K-metal**
371 particle type (3) comprises ~2 % of the particles. It is dominated by a calcium peak at m/z
372 +40 followed by an aluminum peak at m/z +27, a potassium and an iron peak. The peak at
373 m/z +27 could also be attributed to organic carbon e.g. C₂H₃ (Silva & Prather, 2000; Pastor
374 et al., 2003). However, from our EC/TC determination (see 3.3) and the fact that other
375 possible markers OC such as m/z +29, 37, 43, 51 and 63 (Spencer & Prather, 2006) are very
376 weak, we assume the influence of OC to be smaller than from aluminium. The peak at m/z
377 +56 is probably a mixture of Fe and CaO because of the small peak at m/z +57 that indicates

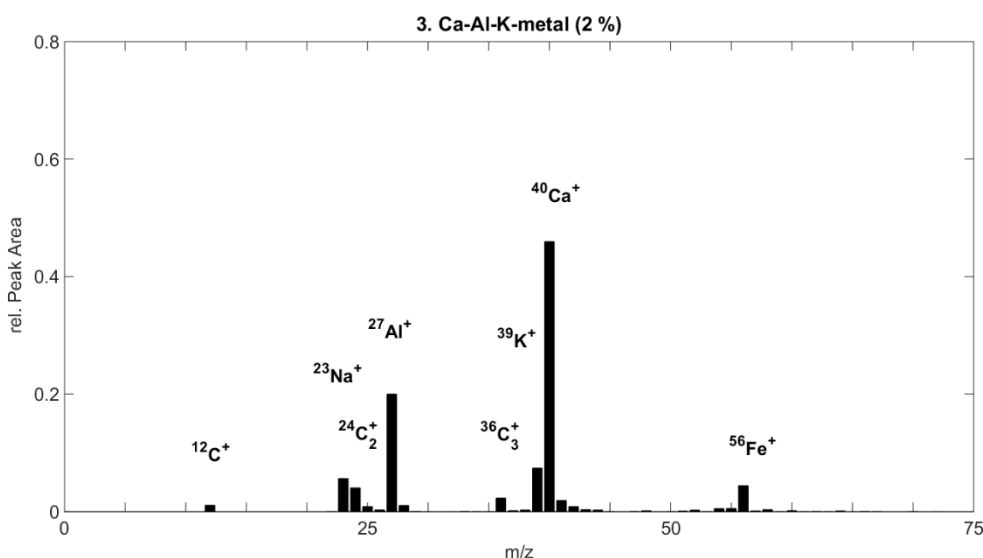
378 the presence of CaOH. The three remaining clusters comprised 16 or less particles each and
379 showed mainly one single peak at $m/z+41$ or $+42$ or $+43$. As a consequence, these clusters
380 were assigned as unclassified.



381



382



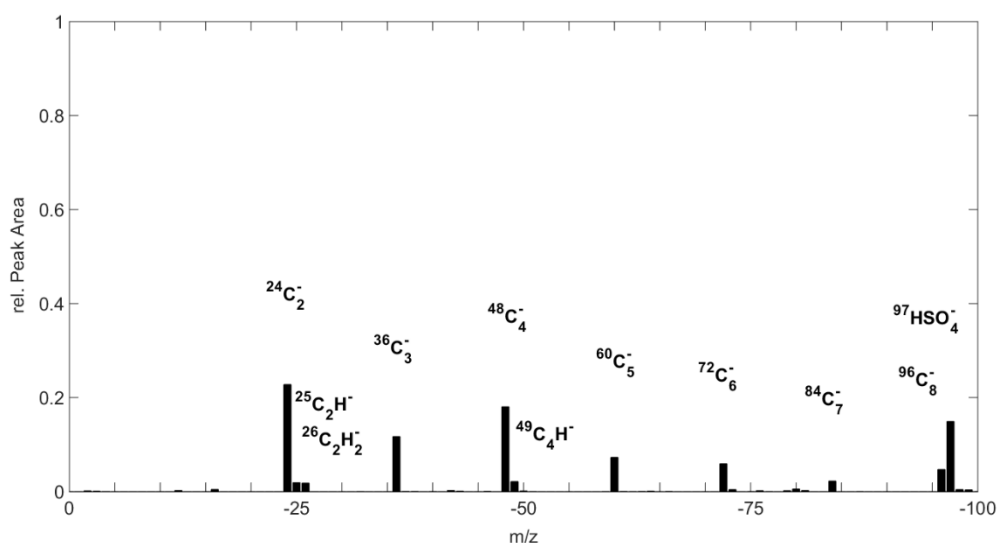
383

384 Figure 3 The three major clusters (i.e. particle types) identified for particles emitted by the CFM56-
 385 7B26/3 engine during A-PRIDE 5.

386

387 By switching the polarities of the ATOFMS' flight tubes, we were able to analyze negatively
 388 charged ions and constituents, though the small number of spectra meant a cluster analysis
 389 was not meaningful. Instead, the average spectrum of the negative ions is presented in Figure
 390 4. Although it cannot be used to identify the individual particle types, it provides insight into
 391 most abundant chemical compounds of the analyzed particles. The average spectrum in
 392 terms of relative peak area mainly shows the presence of EC (peaks at m/z +12, +24, +36,
 393 etc.) and a prominent sulfate signal (m/z +97) which is a typical marker for sulfuric acid. The
 394 average negative spectrum agrees with the positive ions that also indicate a prevailing
 395 presence of EC.

396 Because all three major positive ion clusters indicated the presence of EC, we conclude that
 397 the detected inorganic and metallic compounds were all internally mixed with soot particles.
 398 This is also supported by the average negative spectrum and the fact that only 2.5 % of the
 399 spectra did not show at least one peak associated with EC. Considering that some fraction
 400 of soot can effectively act as INP (Cozic et al., 2008) and that a dominant fraction of ice
 401 residuals in cirrus clouds contain metal compounds (Agrawal et al., 2008) the presented
 402 findings support the assumption that aircraft engine emissions can act as INP.



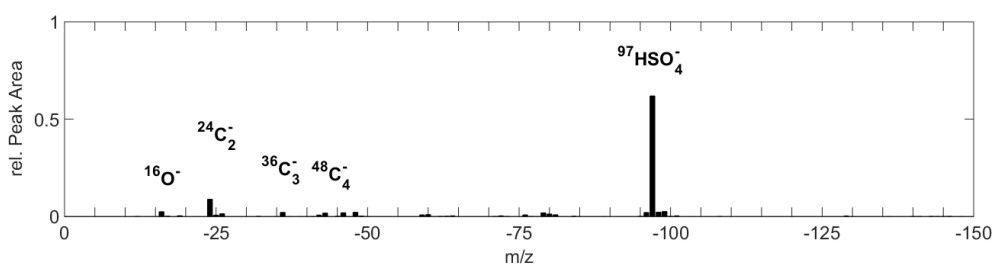
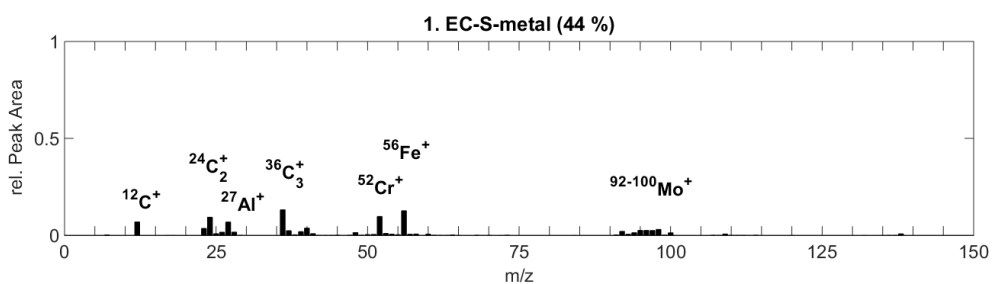
403
404 Figure 4 Average negative spectrum from the spectra collected from the CFM56-7B26/3 engine.

405 3.2.2 CFM56-5B4/P engine

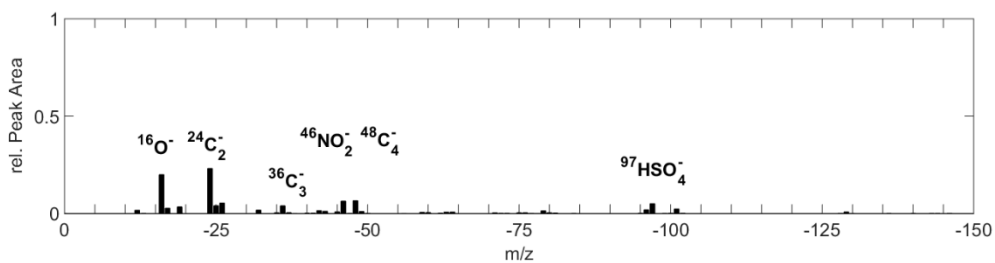
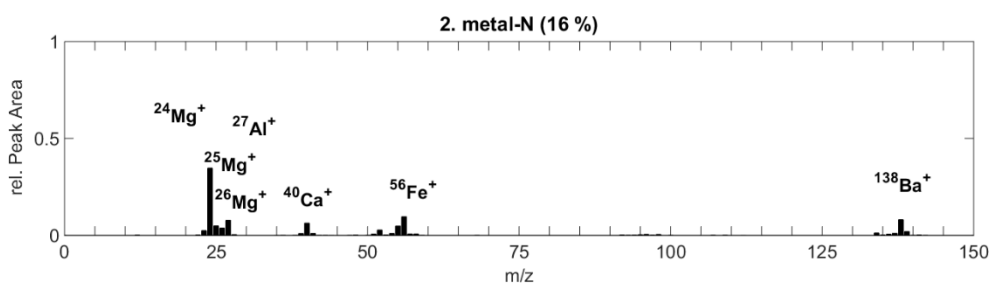
406 The cluster analysis resulted in nine clusters, of which five were considered to represent the
407 main particle types (Figure 5). Although the total number of spectra recorded was only 317,
408 we still discuss the similarities to the particles sampled from the CFM56-7B26/3 engine.

409 The **EC-S-metal** (1) was the most abundant particle type (~44 %). Besides the very
410 prominent sulfate ion peak at $m/z-97$ and the EC pattern, this cluster also shows the presence
411 of metal compounds such as aluminium ($m/z+27$), chromium ($m/z+52$), iron ($m/z+56$) and
412 molybdenum ($m/z+92 - +100$). The **metal-N** particle type (2) is made up from ~16 % of the
413 particles, and shows mainly metal compounds with the most pronounced peaks arising from
414 magnesium ($m/z+24 - +26$), iron, barium ($m/z+138$) and calcium ($m/z+40$). Magnesium
415 was identified due the absence of other EC peaks and the matching isotopic ratio. Nitrate
416 was identified by the peak at $m/z-46$. Here, the EC pattern is only present in the negative
417 spectrum. The **EC-Na-metal** (3) particle type comprises ~25 % of the particles, and is
418 similar to cluster (1). However, this cluster includes a more intense sodium ion peak at m/z
419 $+23$ and a lower intensity of the sulfate peak thus the negative EC pattern is relatively more
420 pronounced. The **Ca-metal-Na-EC** particle type (4) shows combined features of EC, metal
421 compounds and sodium. This cluster comprises ~8 % of all particles, and contrary to the
422 other clusters it shows strong signals of both barium and barium oxide. The peak at $m/z-95$
423 assigned to CH_3SO_3 is ambiguous due to the absence of other peaks from sulfates. Also, this
424 peak has not been observed in other clusters. The peak at $m/z-95$ could potentially be
425 associated with PO_4 or NaCl_2 , however both are unlikely. The presence of phosphate is
426 implausible because no peaks from PO_2 and PO_3 at $m/z-63$ and -79 were detected. For
427 NaCl_2 , an additional peak from its isotopes at $m/z-93$ would be expected. The **EC-S-K-**
428 **metal** particle type (5) comprises ~6 % of the particles. This cluster has very similar features
429 to cluster (1) and (3), despite its dominant sulfate peak at $m/z-96$ instead at $m/z-97$. The
430 spectra of the remaining four clusters make up ~1 % of the total. These clusters all showed

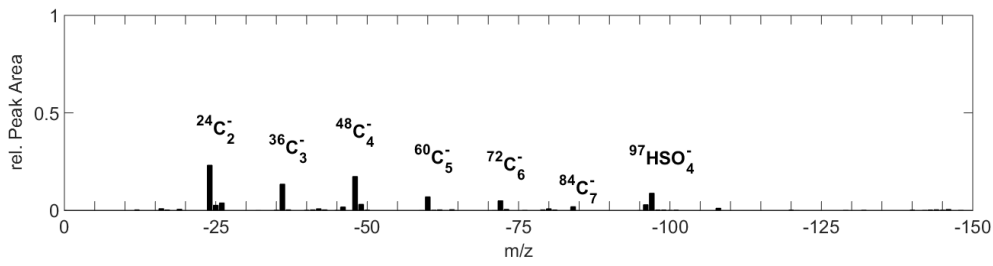
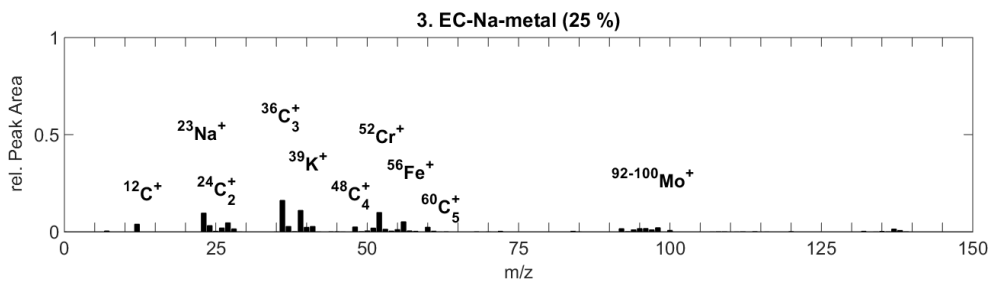
431 peaks associated with EC except for one. This cluster only contained one spectra with a
432 major peak at $m/z+90$ potentially from zirconium and a peak at $m/z-17$ (OH).



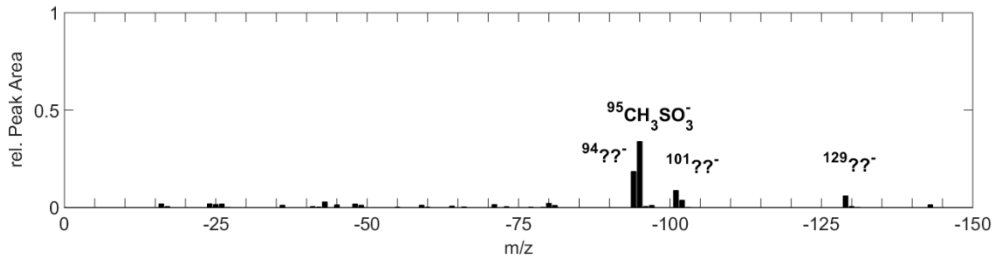
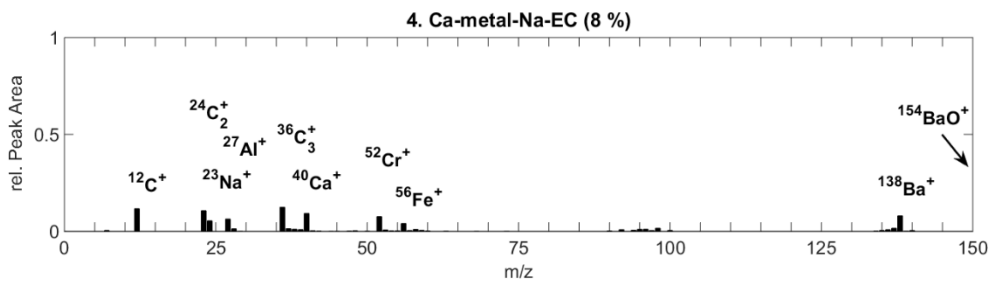
433



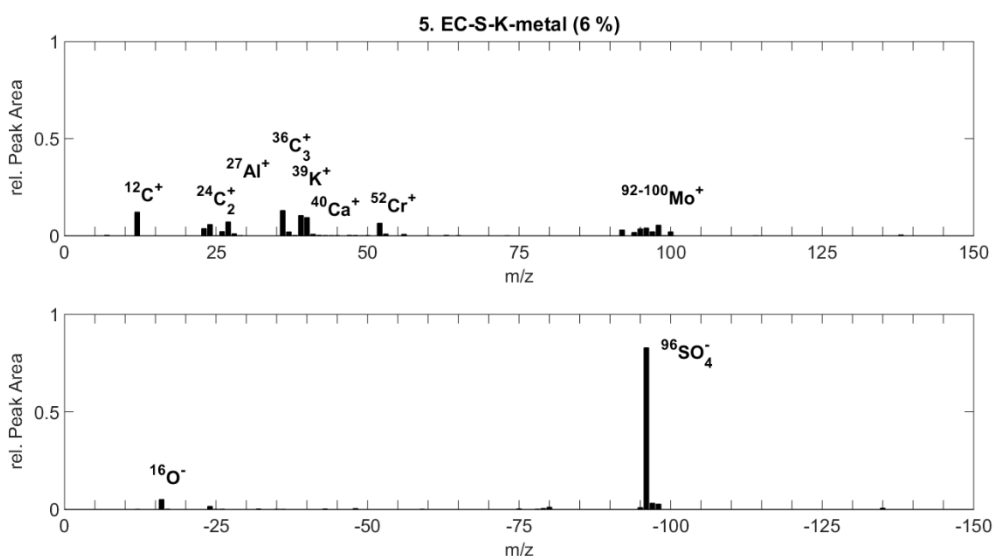
434



435



436



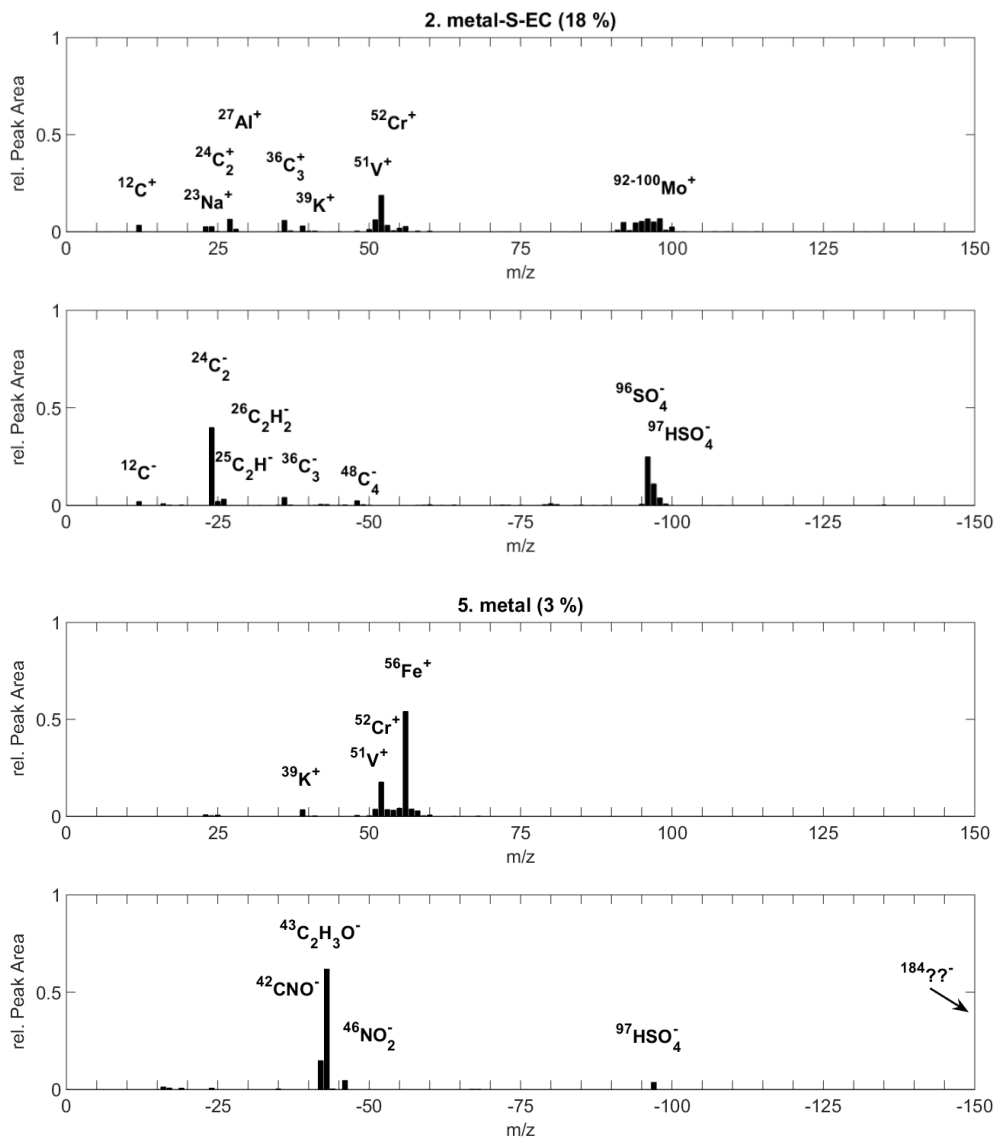
437

438 Figure 5 Cluster analysis from the particle spectra measured from the CFM56-5B4/P engine, including
 439 both positive and negative spectra.

440 3.2.3 CFM56-5C4 engine

441 The cluster analysis of the spectra obtained from the particles emitted by the CFM56-5C4
 442 engine yielded six clusters, three of which already identified for the CFM56-5B4/P engine.
 443 One cluster comprised only one particle. The two new clusters, metal-S-EC cluster (2) and
 444 metal cluster (5), are depicted in Figure 6. The total number of particles chemically analyzed
 445 from the CFM56-5C4 engine was 466.

446 The **EC-Na-metal** (1) particle type was very similar to cluster (3) from the CFM56-5B4/P
 447 engine. Also, contribution by this cluster, 23 %, is comparable. The **metal-S-EC** (2) particle
 448 type comprises 18 % of the particles. This cluster shows similar peaks to cluster (1), with
 449 less pronounced EC and more intense sulfate peaks. Moreover, it has more pronounced peaks
 450 from vanadium ($m/z+51$) and molybdenum ($m/z+92 - +100$). The **EC-S-metal** particle type
 451 (3) looked like cluster 1 from the CFM56-5B4/P engine. Both the clusters comprised the
 452 same number fraction of particles (44 %). The **metal-N** particle type (4) made up of 12 %
 453 of the total particles and was similar to cluster (2) for the CFM56-5B4/P engine with a
 454 distinct presence of barium. The **metal** particle type (5) comprised ~ 3 % of the particles. As
 455 shown, a combination of metal compounds was detected in the positive spectrum, though
 456 the negative spectrum has major peaks that cannot be unambiguously assigned. The peak at
 457 $m/z -43$ is assigned to C_2H_3O thus organic carbon (Spencer & Prather, 2006). The peak at
 458 $m/z -42$ was assigned to CNO, which could emerge due to the simultaneous occurrence of
 459 nitrogen and carbon in the particle (Mauney et al., 1984; Kolaitis et al., 1989). The peak at
 460 $m/z -184$ could not be assigned. This cluster does not have peaks associated with EC in
 461 either of the spectra. The sixth cluster (one spectra) had a dominant sulfate peak at $m/z+97$
 462 and a peak at $m/z-25$ that could not be assigned.



463

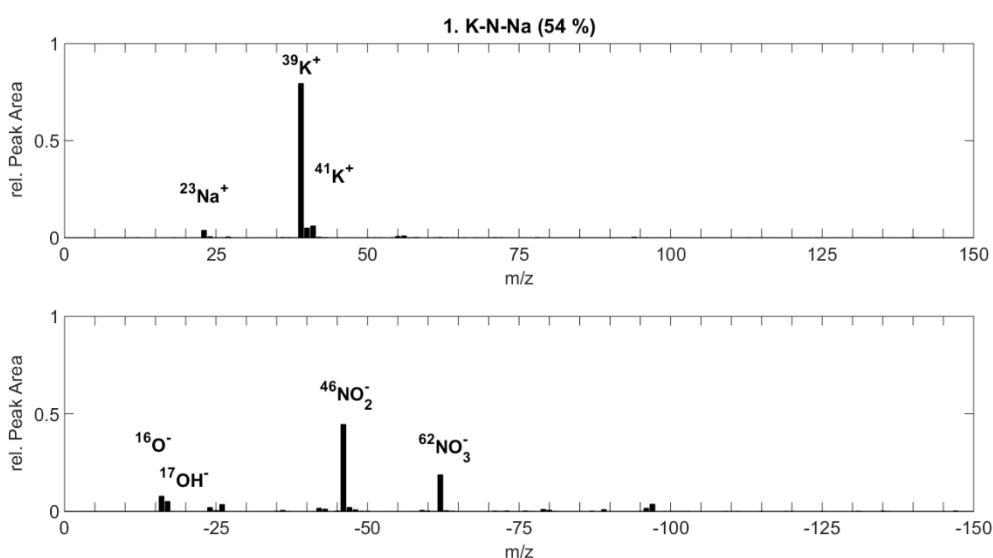
464

465 Figure 6 Cluster analysis from the particle spectra measured from the CFM56-5C4 engine.

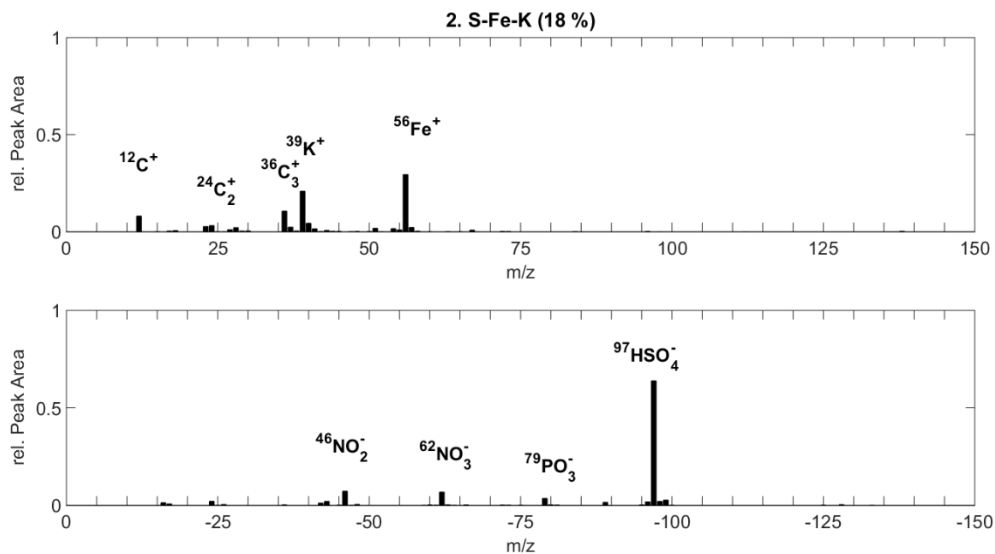
466 3.2.4 Ambient background particles

467 ATOFMS measurements of ambient background particles were conducted in order to
 468 investigate if ambient aerosol particles could influence the engines measurements. The 325
 469 background particles were sampled overnight from 6:00 p.m. to 9:00 a.m. without an engine
 470 running following the test run of the CFM56-5C4 engine which ended at 2:30 p.m. The
 471 sampled particles represent the aerosol particles that enter the test cell with the air that is
 472 consumed by the engine as it is running. During the overnight sampling, the airlocks of the
 473 test cell were left open to allow a passive exchange of the outside air with the test cell air.
 474 The sampling conditions did not fully reflect the situation during engine runs due to the flow
 475 of air through the test cell during engine runs caused by the thrust of the engine.

476 In total, the analysis yielded seven clusters. The two main particle types are displayed in
 477 Figure 7. The **K-N-Na** particle type (1) made up ~54 % of the analyzed particles and has
 478 dominant potassium peaks at m/z +39 and +41 and a smaller sodium peak. Calcium (m/z
 479 +40) is also present though this peak can be the result of the potassium signal at m/z +39
 480 (especially if it is very intense) to which the ATOFMS is very sensitive (Healy et al., 2013)
 481 that sometimes causes a peak to be registered at m/z +40. The negative spectra are dominated
 482 by ion peaks from nitrate at m/z -46 and -62. A likely association with K, Na and N is dust
 483 (Jeong et al., 2011) probably from the road and the freeway nearby. The **S-Fe-K** particle
 484 type (2) comprises ~18 % of the spectra. This cluster is dominated by a strong sulfate (m/z
 485 -97) signal and the presence of iron (m/z +56) and potassium ions (m/z +39). This cluster
 486 also has a weak EC signature in the positive mass spectra. Consequently, these particles
 487 could be aged remainders from aircraft exhaust emitted during previous engine tests or soot
 488 particles from sources nearby. The **K-N-EC** particle type (3) was made up of ~7 % of the
 489 total spectra, and differed from the other clusters by its EC pattern up to C_9^- (m/z -108)
 490 mixed with potassium and nitrate. Additionally, it showed the metal compounds manganese
 491 (m/z +55) and iron (m/z +56). The **Fe-N** particle type (4) comprised ~7 %. In contrast to the
 492 other clusters it displayed a prominent iron peak in the positive spectrum. The negative
 493 spectrum was dominated by a strong nitrate signal and a smaller sulfate peak. The **Ca-N-Na**
 494 particle type (5) comprised ~6 % of the particles. Except for the presence of calcium instead
 495 of potassium, it had similar features than the K-N-Na particle type (1). The **EC-Ca-K-S**
 496 particle type (6) made up ~5 % of the total particles. It depicted low intensities of
 497 carbonaceous peaks from EC mixed with potassium, calcium and sulfate, and in contrast to
 498 the other clusters, phosphate was detected, mainly at m/z -79 (PO_3) and to a smaller extent
 499 at m/z -63 (PO_2). These peaks are commonly associated with soil dust (Silva et al., 2000).
 500 The **K-CN-N** particle type (7) only comprised ~2 % of the total particles. This cluster had a
 501 strong potassium peak in the positive mass spectrum and peaks from organic nitrogen (m/z
 502 -26 (CN), -42 (CNO)) and nitrate (m/z -46, -62) in the negative spectra.



503



504

505 Figure 7 Main clusters from the spectra collected during the ambient background measurements
 506 performed in the test cell without an engine running.

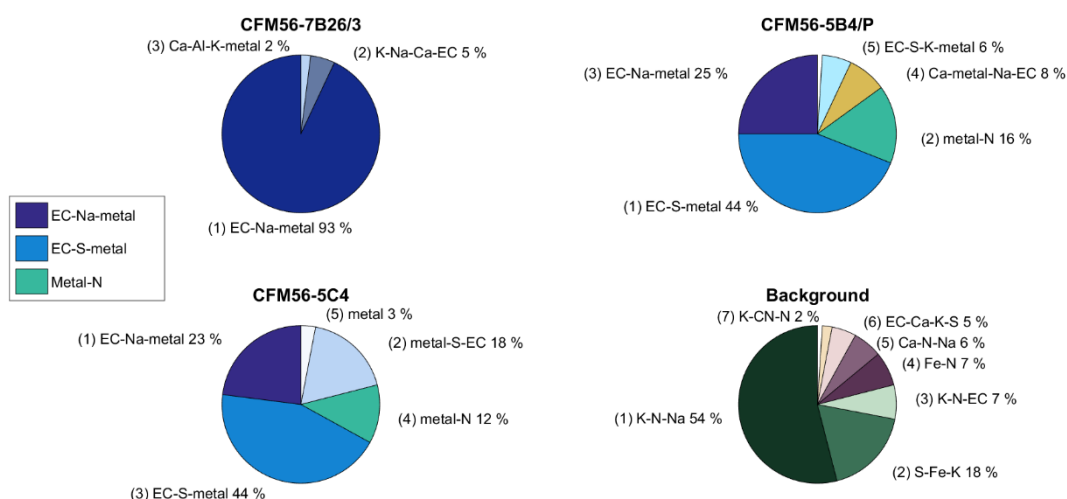
507 3.2.5 Comparison of the identified particle types

508 The particle types identified as described in the previous sections are summarized in Figure
 509 8. The legend depicts the particle types that are detected in more than one engine type. As
 510 mentioned, only small differences were recognized between cluster (1), (3) and (5) from the
 511 CFM56-5B4/P and cluster (1) and (3) from the CFM56-5C4 engine. They are similar to the
 512 EC-Na-metal particle type (cluster 1) presented for the CFM56-7B26/3 engine with respect
 513 to the positive ion spectra. Also, the common particles types from The CFM56-5B4/P and
 514 the CFM56-5C4 engine were similar in terms of number fractions. Together, these particle
 515 types made up more than 75 % of the particles for both engines. These engines mainly
 516 differed from the CFM56-7B26/3 engine because the metal-N particle type was not
 517 observed. However, this is probably due to missing the negative spectra.

518 The analysis of the ambient particles revealed that they do not resemble the exhaust particles
 519 sampled during engine runs. None of the particle types identified for ambient background
 520 aerosol were found in the aircraft exhaust, and only ~12 % of the background particles
 521 depicted a clear EC pattern in both the positive and the negative spectrum. These particles
 522 were assumed to be remainders from previous engine tests or from sources in the vicinity
 523 such as landing and starting aircraft or cars. Most similarities exist between the K-N-EC
 524 (cluster 3) from the ambient background particles and the EC-Na-metal particle type from
 525 the engines, though the K-N-EC particle type clearly differs by the presence of nitrate and
 526 markers for organics. Nitrate however, is found in the metal-N particle type from the aircraft
 527 engines. As all ambient particle types contained nitrate, it is possible that nitrate from
 528 ambient aerosol is partly responsible for the nitrate detected in the particles emitted by the
 529 engines. The opposite is the case for the metallic compounds, especially aluminium,
 530 magnesium, vanadium, chromium, iron, manganese, molybdenum and barium. These are

531 detected in most particle types of the engine emissions but only in cluster 2 and 4 from the
 532 ambient background particles.

533 We conclude that, for metallic compounds the engine emissions have influenced the ambient
 534 background particles and not vice versa. This is also supported by the fact that zirconium
 535 was found in ambient background particles but not in those emitted by the CFM56-7B26/3
 536 engine (see 3.4.1). Moreover, most metal compounds do not vaporize in the engine
 537 combustor according to their boiling points that exceed the maximum combustor
 538 temperature. Thus, the redistribution of the metal compounds from ambient particles onto
 539 the soot particles in the aircraft engine could only happen by coagulation. However, this
 540 would require the metallic compounds to be externally mixed in the ambient aerosol and the
 541 cluster analysis showed that this was not case. Possible exceptions are calcium, sodium, and
 542 magnesium that have boiling points potentially allowing their vaporization within the
 543 combustor. Calcium and sodium are both abundant in ambient atmospheric aerosol and they
 544 possibly can be redistributed from the gas phase onto the soot particles within the engine.
 545 However, considering the large difference in particle concentration between ambient and
 546 exhaust their influence is thought to be minor.



547

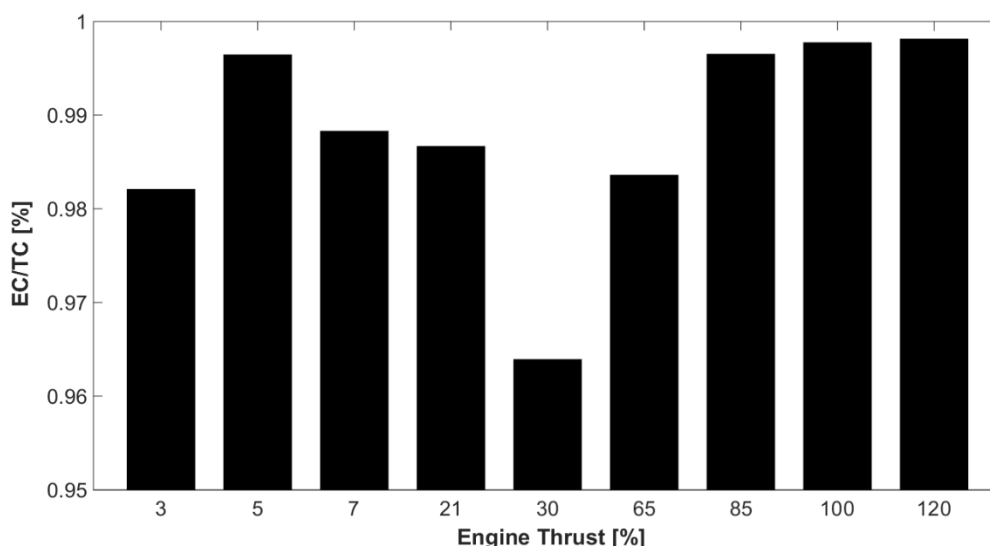
548 Figure 8 Major particle types of the investigated aircraft engines and from the ambient background
 549 aerosol. The number in parentheses is the cluster number as described in the corresponding
 550 chapter.

551 3.3 Elemental Carbon to Total Carbon Ratio

552 Elemental Carbon to Total Carbon (TC) ratios were obtained from positive ATOFMS
 553 spectra by adapting the method presented in Ferge et al. (2006). The thrust-dependent EC/TC
 554 ratios for the CFM56-7B26/3 engine are displayed in Figure 9. The thrust percentage refers
 555 to the predicted thrust at sea level. Depending on the applied thrust, the EC/TC ranged from
 556 0.96 to almost 1. The EC/TC ratios for the emissions from the CFM56-5B4/P and CFM56-
 557 5C4 engines were averaged over all measured thrust levels because the majority of the
 558 spectra were obtained at thrust <30 %. These were 0.89 and 0.83 respectively, considerably

559 lower than for the CFM56-7B26/3 engine. Thus, for this engine the relative contribution of
 560 OC to TC is lower than for the other two engines. We attribute these differences to the
 561 different combustion technologies of the engines. For comparison, Ferge et al. (2006)
 562 reported EC/TC values for soot samples of two different sizes of 0.90 (± 0.05) and 0.89
 563 (± 0.03) from a diffusion flame generator using setting for high organic loadings and 0.94
 564 (± 0.01) and 0.93 (± 0.02) using setting for low organic loadings.

565 For comparison, we calculated the number of particles associated with EC, classed as
 566 particles with peaks at m/z -36, -24, -12, +12, +24 and +36. The number fractions of EC-
 567 containing particles emitted by the CFM56-7B26/3, the CFM56-5B4/P and the CFM56-5C4
 568 engine were 97.5 %, 94.5 % and 96.7 %, respectively. Though the CFM56-5C4 engine is a
 569 mixed flow engine where bypass air is mixed with the exhaust this did not to influence the
 570 fraction of EC-containing particles. This may be explained by the relative low particle
 571 concentration in the bypass air compared to the emitted soot particles.

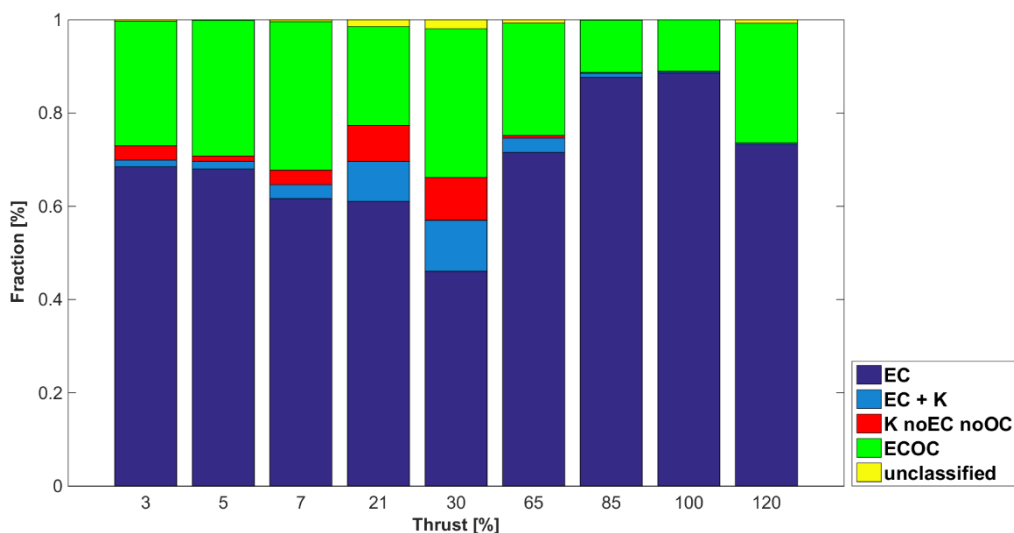


572
 573 Figure 9 Thrust dependent elemental carbon to total carbon values measured by the ATOFMS for the
 574 CFM56-7B26/3 engine.

575 For more detailed information on the carbon-containing particles, MS-Analyze was further
 576 used to classify the particles into ‘EC’ and ‘ECOC’ classes for the CFM56-7B26/3 engine,
 577 depicted in Figure 10 according to the applied thrust. The additional classes, ‘K noEC noOC’
 578 and ‘EC + K’ were used in order to unambiguously identify the ‘ECOC’ class. The ‘K noEC
 579 noOC’ class consisted mainly of spectra from particles that showed a dominant potassium
 580 peak. The number fraction of the ‘ECOC’ class defined in this way has to be considered as
 581 the lower limit because of the possibility that some of the particles from the ‘EC + K’ class
 582 are actually ‘ECOC’.

583 The number fraction of the ‘EC’ class ranges from ~0.5 to ~0.9 % where the highest values
 584 are found to occur in the high thrust range (85 % – 120 %). The ‘K noEC noOC’ class and
 585 ‘unclassified’ particles are the only ones not associated with EC, and were generally higher
 586 at thrust ≤ 30 %. For the same engine type at thrust >30 %, Brem et al. (2015) found that the

587 influence of aromatic species from the Jet A-1 fuel on soot emissions decreases with
 588 increasing thrust. They attributed the observed maximum influence at 30 % thrust to the less
 589 efficient combustion of aromatics, due to lower combustor temperatures and pressures. If
 590 this applies to organics in general, more organic material would remain unburnt at low thrust
 591 than at high thrust, which would explain the generally higher fraction of particles in the ‘EC’
 592 class at higher thrust.



593

594 Figure 10 Thrust dependent fraction of the particles from the CFM56-7B26/3 engine classified into ‘EC’
 595 and ‘ECOC’. The ‘EC+K’ and the ‘K noEC noOC’ classes were needed to define the ‘ECOC’
 596 class.

597 3.4 Metals

598 This section provides information on the abundance of individual metal species that were
 599 detected in the emitted soot particles. This is of importance because metal-containing
 600 particles are shown to potentially act as INP (Cziczo et al., 2013) and thereby impact the
 601 global radiation budget. Moreover, they can cause adverse health effects (Pagan et al., 2003).
 602 Further, we analyzed potential sources of metallic compounds, which include kerosene,
 603 lubricant oil, grease and engine wear. Knowledge of the origin of the individual metallic
 604 compounds is crucial for appropriate attempts to reduce their emissions.

605 3.4.1 Occurrence of metallic compounds

606 The following metallic compounds were detected to be internally mixed with the exhaust
 607 soot particles: molybdenum, calcium, sodium, iron, copper, barium, chromium, aluminium,
 608 silicon, magnesium, cobalt, manganese, vanadium, nickel, lead, titanium and zirconium.
 609 These metallic compounds were detected for all three engines investigated except for
 610 zirconium that was not found in particles from the CFM56-7B26/3 engine. Also, indium,
 611 boron, selenium, arsenic, tin, wolfram, antimony and gadolinium were analyzed, but they
 612 were not detected except for antimony, boron and wolfram that were identified on only four
 613 or less particles each. In general, one or more metallic compounds were detected in a single

614 particle, and the fraction of particles emitted by the CFM56-7B26/3 engine containing at
615 least one, two, three and four metals was 36.3 %, 19.9 %, 10.5 % and 3.2 %, respectively.

616 Although the ATOFMS is a non-quantitative instrument it provides relative peak areas of
617 the identified ions. These give some information on the quantity of chemical species within
618 individual aerosol particles as differences because the matrix effects of the ionization process
619 are minimized by using relative peak areas (Gross et al., 2000). The metals, number fractions
620 and peak areas are listed in Table 1. The fractions are sorted according to the applied thrust
621 to reveal variations between the different phases during the flight of an aircraft. The relative
622 peak area value given in parenthesis is normalized for each metallic compound so that the
623 largest peak area measured corresponds to 1 for that metal. The number fraction of particles
624 containing the individual metallic compound emitted by the CFM56-5C4 and the CFM56-
625 5B4/P engine and sampled from the ambient background measurements. The data for these
626 two engines were averaged over all measured thrusts because not enough particles were
627 sampled for a thrust-dependent analysis. However, ~80 % of these particles were sampled at
628 thrusts <30 % corresponding largely to the low thrust range.

629 For the CFM56-7B26/3 engine the fraction of particles containing molybdenum is largest at
630 the high thrust range. Also within this range, the fraction was found to increase with
631 increasing thrust. For calcium, sodium, iron, copper and barium the corresponding fractions
632 of particles containing the metal are largest at low thrust and decrease with increasing thrust.
633 A reason for this behavior could be the increasing total particle concentration with increasing
634 thrust. If the total amount of these metallic compounds did not increase with increasing
635 thrust, then relatively less particles are affected by them. For chromium, aluminium, silicon,
636 magnesium, cobalt, vanadium, nickel, lead and titanium the corresponding fractions of
637 particles containing the metal are largest at medium thrust. In contrary to the other
638 compounds the peak area values from calcium and barium are not largest at that thrust range
639 where the fraction of calcium- and barium-containing particles are largest. This indicates
640 that the amount of calcium and barium present on each particle is largest at medium thrust
641 despite the smaller number fractions.

642 The fractions of metal-containing particles were generally higher for the CFM56-5B4/P and
643 the CFM56-5C4 than for the CFM56-7B26/3 engine with the largest differences found for
644 molybdenum, barium, chromium, aluminium, manganese, magnesium, vanadium, nickel
645 and lead. As discussed in the next section, kerosene, lubricant oil, grease and engine wear
646 are potential sources of these metals. One reason for the larger fractions is the possible
647 difference in oil and grease consumption. The CFM56-5B4/P and the CFM56-5C4 engine
648 generally have a higher oil consumption than the CFM56-7B26/3 engine. Another reason
649 for the differences in the measured metal-containing fractions are variations thereof over
650 time for the same engine. Alloys sometimes consist of heterogeneously distributed
651 compounds. Thus, if wear takes place and an engine alloy frets, its individual compounds
652 are unevenly released.

653 The presented fractions of particles that contain metallic compounds are lowest for the
654 ambient background particles except for silicon, lead and aluminium of which the latter
655 shows similar values than the CFM56-7B26/3 engine. It is likely that the ambient

656 background measurements were influenced by previous engine test runs, especially by the
 657 last test run engine beforehand conducted on the CFM56-5C4.

658 Table 1 Number fraction in percent of spectra from particles emitted by the CFM56-7B26/3, the CFM56-
 659 5C4, the CFM56-5B4/P engine and from ambient background showing peaks indicating the
 660 presence of the corresponding metal compound. For the CFM56-7B26/3 engine the values are
 661 pooled into low (3 % – 7 %, idle/taxi), medium (20 % – 65 %, cruise) and high (85 % – 120 %,
 662 take-off) thrust range, and the value in parenthesis is the average peak area normalized to the
 663 largest value for each metal.

| Element | CFM56-7B26/3 | | | CFM56-5C4 | CFM56-5B4/P | Background |
|------------|--------------|---------------|-------------|-----------|-------------|------------|
| | Low thrust | Medium thrust | High thrust | | | |
| Molybdenum | 5.3 (0.52) | 5.9 (0.73) | 9.6 (1.00) | 55.9 | 36.7 | 1.9 |
| Calcium | 32.4 (0.61) | 16.2 (1.00) | 1.8 (0.04) | 22.3 | 39.1 | 23.1 |
| Sodium | 29.1 (1.00) | 22.6 (0.41) | 4.3 (0.06) | 50.2 | 51.1 | 34.5 |
| Iron | 22.5 (1.00) | 8.4 (0.49) | 0.7 (0.06) | 33.0 | 35.5 | 11.1 |
| Copper | 2.9 (1.00) | 0.4 (0.50) | 0.0 (—) | 2.6 | 6.7 | 2.5 |
| Barium | 0.5 (0.16) | 0.3 (1.00) | 0.1 (0.08) | 3.7 | 16.5 | 2.2 |
| Chromium | 2.7 (0.10) | 17.2 (1.00) | 3.6 (0.18) | 72.3 | 52.0 | 5.2 |
| Aluminium | 3.1 (0.21) | 8.4 (1.00) | 1.0 (0.03) | 8.3 | 13.5 | 15.1 |
| Silicon | 0.4 (0.36) | 2.1 (1.00) | 0.1 (0.15) | 0.2 | 0.9 | 4.3 |
| Magnesium | 0.6 (0.46) | 1.7 (1.00) | 0.3 (0.04) | 16.6 | 20.8 | 3.1 |
| Cobalt | 0.5 (0.83) | 1.4 (1.00) | 0.4 (0.93) | 1.7 | 2.8 | 1.5 |
| Manganese | 0.3 (0.84) | 0.9 (1.00) | 0.1 (0.02) | 17.5 | 17.4 | 8.9 |
| Vanadium | 0.4 (0.89) | 0.7 (1.00) | 0.1 (0.04) | 9.4 | 9.2 | 3.4 |
| Nickel | 0.4 (0.12) | 0.6 (1.00) | 0.1 (0.04) | 10.7 | 19.3 | 8.3 |
| Lead | 0.1 (0.36) | 0.4 (1.00) | 0.0 (—) | 1.3 | 0.9 | 2.5 |
| Titanium | 0.0 (—) | 0.2 (1.00) | 0.0 (—) | 0.0 | 0.9 | 0.0 |
| Zirconium | 0.0 (—) | 0.0 (—) | 0.0 (—) | 0.9 | 0.6 | 0.3 |

664 3.4.2 Potential Sources of Metals

665 ICP-MS was conducted to investigate potential sources of the metallic compounds identified
 666 in the exhaust particles of aircraft engines. It was applied as quantitative element screening

667 on a) kerosene (Jet A-1 Fuel), b) engine lubricant oil (Mobile Jet II) and c) engine wear
668 collected from debris within the engine.

669 Kerosene and oil samples were taken from the batch actually consumed by the aircraft engine
670 during the A-PRIDE 5 campaign. As a reference for material from engine wear, a sample of
671 debris collected on the blades of the High Pressure Turbine (HPT) of another CFM-7B
672 engine type was used. The HPT is located downstream of the combustor where the collected
673 debris was carried and accumulated by combustor air. The influence of oil on the emissions
674 is thought to be less important compared to kerosene because of the much smaller amounts
675 consumed. The ratio of kerosene to oil consumption is estimated to be $\sim 5000 \pm 1500$ for a
676 CFM engine at cruise condition. Another potential source of the identified metal compounds
677 in the exhaust not analyzed herein is grease mainly applied to rotating engine parts.

678 The detection of silicon in kerosene and oil samples using ICP-MS was not possible because
679 of the analytical procedure applied. The concentrations in milligram per kilogram [mg/kg]
680 of the most abundant metallic elements in Mobile Jet A-1 Fuel and Mobile Jet II Oil are
681 shown in Table 2. ‘Others’ comprise compounds with >0.1 mg/kg each, including barium,
682 manganese, arsenic, tin, nickel and molybdenum detected in both fuel and oil, whereas
683 indium and boron were solely detected in fuel, and selenium solely in oil. Besides the
684 metallic elements, sulphur and phosphor were also detected in both samples.

685 Table 2 Concentrations in milligram per kilogram [mg/kg] of the most abundant metallic elements in
686 Mobile Jet A-1 Fuel and Mobile Jet II Oil detected using ICP-MS.

| Element | Mobile Jet A-1 Fuel | Mobile Jet II Oil |
|-----------|---------------------|-------------------|
| Calcium | 113.15 | 30.82 |
| Vanadium | 3.59 | 1.82 |
| Aluminium | 3.08 | 4.35 |
| Lead | 1.98 | >0.1 |
| Iron | 1.69 | 1.77 |
| Magnesium | 1.46 | 2.25 |
| Titanium | 1.45 | 6.01 |
| Sodium | 1.05 | 1.28 |
| Copper | 0.96 | (—) |
| Antimony | >0.1 | 1.15 |
| Chromium | (—) | 1.09 |
| Others | 4.91 | 5.3 |

687 The elements that were detected in the solid HPT debris using ISP-MS are shown in Table
688 3 in percentage of mass [wt%]. It only lists the elements detected in the exhaust particles as

689 well, covering 98.2 % of the mass of the HPT debris sample. The debris was stored in 95 %
 690 ethanol and 5 % isopropyl alcohol after sampling and a potential contamination from the
 691 solvent cannot be excluded. The suspension was homogenized and dried directly before the
 692 analysis.

693 Table 3 Mass fractions in percentage of mass [wt%] and 95 % Confidence Intervals (CI) of elements in
 694 solid residue from the HPT debris obtained using ICP-MS.

| Element | Massfraction, CI (95 %) |
|----------------|--------------------------------|
| Silicon | 60.1, [59.6, 60.6] |
| Calcium | 12.2, [11.4, 13.0] |
| Sodium | 5.03, [4.88, 5.18] |
| Iron | 5.00, [4.65, 5.35] |
| Aluminium | 4.90, [4.60, 5.20] |
| Magnesium | 4.00, [3.90, 4.10] |
| Nickel | 3.43, [3.39, 3.47] |
| Chromium | 0.90 [0.86, 0.94] |
| Titanium | 0.63 [0.61, 0.65] |
| Manganese | 0.39 [0.39, 0.40] |
| Lead | 0.39 [0.37, 0.41] |
| Copper | 0.48 [0.45, 0.51] |
| Cobalt | 0.32 [0.32, 0.33] |
| Barium | 0.20 [0.17, 0.23] |
| Molybdenum | 0.18 [0.17, 0.19] |
| Vanadium | 0.051 [0.049, 0.053] |
| Zirconium | 0.017 [0.012, 0.022] |

695 The ICP-MS of the HPT debris was used to reveal compounds that are probably from engine
 696 wear. Although the identified compounds were part of the combustion air, the actual
 697 composition of the HPT debris as it was collected has not contributed to the combustion
 698 process like kerosene and oil. From empirical values the HPT debris was accumulated in the
 699 engine over an estimated engine operation time of about 20 000 hours to 30 000 hours.
 700 During this time, huge amounts of air passed through the HPT, allowing the accumulation
 701 of compounds not only from engine processes such as wear or kerosene and oil residues and

702 but probably also from ambient aerosol collected during flight. We assume silicon, calcium
703 and sodium from ambient to cause the large weight fractions of in the HPT debris.

704 A potential source of aircraft engine wear are the so-called honeycomb structures that are
705 built into in the compressor region of the engine downstream the combustor. The honeycomb
706 structures are a wearing part made out of 'Hastelloy X'. The chemical composition and the
707 corresponding weight fractions in percentages (in parenthesis) according to the specification
708 sheet (Haynes, 1997) is: Ni (47), Cr (22), Fe (18), Mo (9), Co (1.5), W (0.6), Mn (≤ 1), Si
709 (≤ 1), B (≤ 0.008). It was suggested that wear from 'Hastelloy X' contribute to debris collected
710 in the HPT. However, the relative large amounts of molybdenum in 'Hastelloy X' and the
711 large fractions of exhaust particles containing molybdenum are not reflected in the small
712 mass fraction of molybdenum found in HPT debris. Thus, the amount of 'Hastelloy X' in
713 HPT debris is probably rather small. Nevertheless, this does not exclude the possibility of
714 wear from 'Hastelloy X' to contribute to the metals identified in the exhaust particles. Below,
715 we discuss potential sources for each individual metal compound identified in the emitted
716 engine particles based on the ICP-MS analyses.

717 **Exclusively engine wear:**

718 **Zirconium** was detected in small amounts in HPT debris but not in kerosene or oil. It is
719 known to be used as thermal barrier coating in aircraft engine parts (Miller, 1997). **Cobalt**
720 was detected in small amounts in HPT debris and it is used in 'Hastelloy X' but not in
721 kerosene or oil.

722 **Mainly engine wear:**

723 **Iron** was detected in substantial amounts in HPT debris and in 'Hastelloy X'. It was also
724 found in kerosene and in oil. Compared to other metallic compounds such as vanadium, lead,
725 magnesium and titanium the number fraction of iron-containing particles was relatively high
726 whereas the amounts detected in kerosene and oil were similar. Thus, we assume this
727 difference in the fraction to be caused by the higher iron content in HPT debris and in
728 'Hastelloy X'. **Copper** was detected in kerosene and it is used in 'Hastelloy X'. Copper was
729 not detected in oil. It was detected in the exhaust particles mainly in combination with iron
730 indicating engine wear as a major source. **Chromium** was detected in HPT debris and
731 'Hastelloy X' contains a weight fraction of 22 %. Chromium is widely used in engine parts
732 e.g. aircraft turbine blades and alloys. It was detected in oil but not in kerosene. **Nickel** is
733 the most abundant constituent of 'Hastelloy X' and it shows a substantial weight fraction of
734 3.4 % in HPT debris. Only very low concentrations of nickel were detected in kerosene and
735 in oil. **Molybdenum** is a main constituent of 'Hastelloy X'. However, in aerospace,
736 molybdenum disulfide is widely used in grease for lubricant applications where metal to
737 metal contact exists. It can be converted directly to molybdenum metal when heated
738 (Epshteyn & Risdon, 2010). The highest number fraction of molybdenum-containing
739 particles was measured at maximum thrust when grease consumption and engine wear are
740 likely to be highest. Only small quantities were detected in kerosene and oil. We therefore
741 assume molybdenum to originate mainly from engine wear and grease.

742 **Mainly kerosene:**

743 **Barium** was detected in kerosene and in oil. It is not supposed to be present in any engine
744 parts. As a side note, it was earlier used in kerosene as a nucleation core for soot in order to
745 reduce the smoke number. **Vanadium** was detected in kerosene and in oil. Engine wear as
746 source of vanadium is not significant due to the very small amount detected in HPT debris.
747 **Lead** was mainly detected in kerosene and only small amounts were detected in oil and in
748 HPT debris. Lead is not used in any engine parts. **Titanium** was detected in kerosene and in
749 oil. Small amount were also detected in HPT debris may be from alloys used in the
750 compressor of aircraft engine upstream of the combustor. **Calcium** and **sodium** were both
751 detected in kerosene and in oil. Especially calcium was detected in relatively large
752 concentrations. Both kerosene and oil probably contribute to their existence in the exhaust
753 particles. Calcium and sodium originating from engine wear can be excluded because they
754 are not used in any engine part. However, ambient aerosol as an additional source is also
755 possible because of the large fraction of ambient background particles containing calcium
756 and/or sodium and the possibility that these compounds are redistributed onto the exhaust
757 particles via gas phase processes.

758 **No main source identified:**

759 **Aluminium** was detected in kerosene, in oil and in HPT debris. Also, it is used in many
760 engine parts. **Silicon** could not be searched for using the ICP-MS method applied to the
761 kerosene and oil samples. Small amounts of silicon are used in many materials used in
762 aircraft engines. **Magnesium** was detected in oil, kerosene and HPT debris which are all
763 potential sources. **Manganese** was detected in small amounts in oil, kerosene and HPT
764 debris. Similar to silicone, it is commonly present in engine parts.

765 4 Summary and Conclusions

766 We investigated the chemical composition of single particles from three different aircraft
767 engine emissions using an ATOFMS. Namely, a CFM56-7B26/3, a CFM56-5B4/P and a
768 CFM56-5C4 turbine were investigated. The CFM56 series are high-bypass turbofan engines.
769 The CFM56-7B26/3 and the CFM56-5B4/P are core flow engines whereas the CFM56-5C4
770 is a mixed flow engine. Particle types were identified using a data mining software enabling
771 the analysis of atmospheric mass spectra. The bulk EC/TC ratios were determined.
772 Furthermore, we determined the fractions of particles that contained metallic compounds. In
773 order to identify sources of the metallic compounds ICP-MS was performed on samples from
774 Jet A-1 fuel, Mobile Jet II and engine wear debris. The particles that were analyzed by the
775 ATOFMS represented a subset of the non-volatile emissions composing only the largest
776 particles due to instrumental restrictions.

777 Depending on engine type, 94.5 % to 97.5 % of the particles contained EC. Particles were
778 grouped into particle types according to their chemical compositions and interpreted. The

779 particle types emitted by all three engine types showed similar chemical composition and
780 number fractions. The thrust-dependent TC/EC ratio of the emissions from the CFM56-
781 7B26/3 engine ranged from 0.96 up to more than 0.99 depending on the applied thrust. The
782 TC/EC ratio of the emissions from the CFM56-5B4/P and the CFM56-5C4 engine were 0.89
783 and 0.83, respectively. These results were not influenced by whether the engine was a core
784 flow engine or a mixed flow engine.

785 Particles containing metallic compounds were all internally mixed with the soot. The
786 following compounds were detected in particles from all engines: Cr, Fe, Mo, Na, Ca, Al,
787 V, Ba, Co, Cu, Ni, Pb, Mg, Mn, Si and Ti. Zr was only detected for the CFM56-5B4/P and
788 the CFM56-5C4 engine. The fraction of metal-containing particles was lower for the
789 CFM56-7B26/3 engine than for the CFM56-5B4/P and the CFM56-5C4 engine. To identify
790 sources of the metallic compounds ICP-MS analyses were carried out. Traces of all
791 compounds were detected in kerosene and/or in oil except for Co and Zr. We conclude that
792 cobalt and zirconium can possibly be used as tracers for aircraft exhaust because they solely
793 originate from engine wear. This accounts especially for cobalt because it was detected in
794 the emission from all of three engines investigated. However, this would require further
795 research because other combustion sources of cobalt- and zirconium-containing soot
796 particles cannot be completely excluded. Nevertheless, the usage of cobalt and zirconium is
797 rather limited. To use the other detected compounds as tracers is not possible because diesel
798 and petroleum are produced from crude oil just like kerosene. Thus, the metallic compounds
799 detected in kerosene can be expected to be found in other fuels and emissions, too.

800 In general, an unambiguous source apportionment of the metal compounds detected in the
801 engine exhaust particles is difficult because of multiple reasons. Most importantly, many
802 metals are detected at least in small amounts in multiple potential sources. Further, it is
803 difficult to quantitatively relate the sources to the compounds detected in the particles. On
804 the one hand, the relative extents of the contribution from the individual sources are not
805 exactly known. This is partly because aircraft engines are a complex system where
806 exploration of chemo physical processes of trace elements within the engine is difficult
807 because no direct observations are possible. On the other hand, the ATOFMS data is non-
808 quantitative and represent only the largest exhaust particles. Moreover, engine wear and oil
809 and grease consumption are not constant over the lifetime of an aircraft engine.

810 The implications of our results are of importance due to the potential of metal-containing
811 particles to act as INP and consequently impact cirrus cloud properties and thus global
812 climate (Cziczo et al., 2013). As a minimum value among the three engines, 36 % of the
813 particles emitted by the CFM56-7B26/3 engine contained at least one metallic compound. If
814 this applies to the smaller particles as well, these finding suggest that aircraft engine
815 emissions are a considerable source of potential INP in the atmosphere. The assumption that
816 smaller particles show similar chemical composition than larges ones is supported by the
817 fractions of metal-containing particles which did not show a size-dependence in our
818 investigated size-range. Also, Demirdjian et al. (2007) has not observed appreciable
819 differences in the chemical composition between small and large soot particles sampled
820 directly behind an aircraft gas turbine engine. The majority of the actual aircraft emissions

821 take place in the upper troposphere where they mainly are at cruise condition that
822 corresponds to the herein presented medium thrust range. Our thrust-dependent analysis
823 revealed that for most of the metallic compounds, the measured averaged relative peak areas
824 were found to be largest at medium thrust. This indicates that also their contents in the soot
825 particles are largest at medium thrust. If the presence of a metallic compound is responsible
826 for the IN activity of a soot particle, a larger content probably enhances its effectiveness to
827 act as INP. At medium thrust range, measurements of the emissions showed high particle
828 concentrations of $>10^6 \text{ cm}^{-3}$ (Abegglen et al., 2015) for the CFM56-7B26/3 engine. In the
829 upper troposphere the concentration of INP is typically in the order of $<0.01 \text{ cm}^{-3}$ (P. J.
830 DeMott et al., 2003) where additional INP would contribute substantially to the total number,
831 potentially resulting in significant cirrus modifications (Hendricks et al., 2005). Therefore,
832 to understand the connection between metal-containing particles from aircraft exhaust and
833 ice nucleation, we recommend investigation of the ice-nucleating properties of non-volatile
834 aircraft emissions.

835 References

- 836 Abegglen, M., L. Durdina, B. T. Brem, J. Wang, T. Rindlisbacher, J. C. Corbin, et al., 2015:
837 Effective density and mass–mobility exponents of particulate matter in aircraft
838 turbine exhaust: Dependence on engine thrust and particle size. *Journal of Aerosol*
839 *Science*, **88**, 135-147. doi: <http://dx.doi.org/10.1016/j.jaerosci.2015.06.003>
- 840 Agrawal, H., A. A. Sawant, K. Jansen, J. Wayne Miller, & D. R. Cocker Iii, 2008:
841 Characterization of chemical and particulate emissions from aircraft engines.
842 *Atmospheric Environment*, **42**(18), 4380-4392. doi:
843 <http://dx.doi.org/10.1016/j.atmosenv.2008.01.069>
- 844 Boies, A. M., M. E. J. Stettler, J. J. Swanson, T. J. Johnson, J. S. Olfert, M. Johnson, et al.,
845 2015: Particle Emission Characteristics of a Gas Turbine with a Double Annular
846 Combustor. *Aerosol Science and Technology*, **49**(9), 842-855. doi:
847 10.1080/02786826.2015.1078452
- 848 Braun, A., F. E. Huggins, S. Seifert, J. Ilavsky, N. Shah, K. E. Kelly, et al., 2004: Size-range
849 analysis of diesel soot with ultra-small angle X-ray scattering. *Combustion and*
850 *Flame*, **137**(1–2), 63-72. doi: <http://dx.doi.org/10.1016/j.combustflame.2004.01.003>
- 851 Brem, B., L. Durdina, F. Siegerist, P. Beyerle, K. Bruderer, T. Rindlisbacher, et al., 2015:
852 Effects of fuel aromatic content on non-volatile particulate emissions of an in-
853 production aircraft gas turbine. *Environmental Science & Technology*. doi:
854 10.1021/acs.est.5b04167
- 855 Burkhardt, U., & B. Kärcher, 2011: Global radiative forcing from contrail cirrus. *Nature*
856 *Climate Change*, **1**, 54-58. doi: 10.1038/nclimate1068
- 857 Corporan, E., A. Quick, & M. J. DeWitt, 2008: Characterization of particulate matter and
858 gaseous emissions of a C-130H aircraft. *J Air Waste Manag Assoc*, **58**(4), 474-483.

- 859 Cozic, J., S. Mertes, B. Verheggen, D. J. Cziczo, S. J. Gallavardin, S. Walter, et al., 2008:
 860 Black carbon enrichment in atmospheric ice particle residuals observed in lower
 861 tropospheric mixed phase clouds. *Journal of Geophysical Research: Atmospheres*,
 862 **113**(D15), n/a-n/a. doi: 10.1029/2007JD009266
- 863 Cziczo, D. J., K. D. Froyd, C. Hoose, E. J. Jensen, M. Diao, M. A. Zondlo, et al., 2013:
 864 Clarifying the Dominant Sources and Mechanisms of Cirrus Cloud Formation.
 865 *Science*, **340**(6138), 1320-1324. doi: 10.1126/science.1234145
- 866 Cziczo, D. J., O. Stetzer, A. Worringer, M. Ebert, S. Weinbruch, M. Kamphus, et al., 2009:
 867 Inadvertent climate modification due to anthropogenic lead. *Nature Geosci*, **2**(5),
 868 333-336. doi:
 869 http://www.nature.com/ngeo/journal/v2/n5/supinfo/ngeo499_S1.html
- 870 DeCarlo, P. F., J. G. Slowik, D. R. Worsnop, P. Davidovits, & J. L. Jimenez, 2004: Particle
 871 Morphology and Density Characterization by Combined Mobility and Aerodynamic
 872 Diameter Measurements. Part 1: Theory. *Aerosol Science and Technology*, **38**, 1185-
 873 1205. doi: 10.1080/027868290903907
- 874 Demirdjian, B., D. Ferry, J. Suzanne, O. B. Popovicheva, N. M. Persiantseva, & N. K.
 875 Shonija, 2007: Heterogeneities in the Microstructure and Composition of Aircraft
 876 Engine Combustor Soot: Impact on the Water Uptake. *Journal of Atmospheric*
 877 *Chemistry*, **56**(1), 83-103. doi: 10.1007/s10874-006-9043-9
- 878 DeMott, P. J., 1990: An Exploratory Study of Ice Nucleation by Soot Aerosols. *Journal of*
 879 *Applied Meteorology*, **29**(10), 1072-1079. doi: 10.1175/1520-
 880 0450(1990)029<1072:AESOIN>2.0.CO;2
- 881 DeMott, P. J., D. J. Cziczo, A. J. Prenni, D. M. Murphy, S. M. Kreidenweis, D. S. Thomson,
 882 et al., 2003: Measurements of the concentration and composition of nuclei for cirrus
 883 formation. *Proceedings of the National Academy of Sciences*, **100**(25), 14655-14660.
 884 doi: 10.1073/pnas.2532677100
- 885 Diehl, K., & S. K. Mitra, 1998: A laboratory study of the effects of a kerosene-burner exhaust
 886 on ice nucleation and the evaporation rate of ice crystals. *Atmospheric Environment*,
 887 **32**(18), 3145-3151. doi: [http://dx.doi.org/10.1016/S1352-2310\(97\)00467-6](http://dx.doi.org/10.1016/S1352-2310(97)00467-6)
- 888 Duda, D. P., P. Minnis, K. Khlopenkov, T. L. Chee, & R. Boeke, 2013: Estimation of 2006
 889 Northern Hemisphere contrail coverage using MODIS data. *Geophysical Research*
 890 *Letters*, **40**(3), 612-617. doi: 10.1002/grl.50097
- 891 Durdina, L., B. T. Brem, M. Abegglen, P. Lobo, T. Rindlisbacher, K. A. Thomson, et al.,
 892 2014: Determination of PM mass emissions from an aircraft turbine engine using
 893 particle effective density. *Atmospheric Environment*, **99**, 500-507. doi:
 894 10.1016/j.atmosenv.2014.10.018
- 895 Epshteyn, Y., & T. J. Risdon, 2010: Molybdenum disulfide in lubricant applications – a
 896 review. In: The 12 lubricating grease conference (NLGI-India Chapter) (pp. 1-12).
 897 Goa, India.
- 898 Ferge, T., E. Karg, A. Schröppel, K. R. Coffee, H. J. Tobias, M. Frank, et al., 2006: Fast
 899 Determination of the Relative Elemental and Organic Carbon Content of Aerosol
 900 Samples by On-Line Single-Particle Aerosol Time-of-Flight Mass Spectrometry.
 901 *Environmental Science & Technology*, **40**, 3327-3335. doi: 10.1021/es050799k
- 902 Gard, E., J. E. Mayer, B. D. Morrical, T. Dienes, D. P. Fergenson, & K. A. Prather, 1997:
 903 Real-Time Analysis of Individual Atmospheric Aerosol Particles: Design and

- 904 Performance of a Portable ATOFMS. *Analytical Chemistry*, **69**(20), 4083-4091. doi:
905 10.1021/ac970540n
- 906 Giorio, C., A. Tapparo, M. Dall'Osto, R. M. Harrison, D. C. S. Beddows, C. Di Marco, et
907 al., 2012: Comparison of three techniques for analysis of data from an Aerosol Time-
908 of-Flight Mass Spectrometer. *Atmospheric Environment*, **61**, 316-326. doi:
909 10.1016/j.atmosenv.2012.07.054
- 910 Gross, D. S., R. Atlas, J. Rzeszutarski, E. Turetsky, J. Christensen, S. Benzaid, et al., 2010:
911 Environmental chemistry through intelligent atmospheric data analysis.
912 *Environmental Modelling & Software*, **25**(6), 760-769. doi:
913 <http://dx.doi.org/10.1016/j.envsoft.2009.12.001>
- 914 Gross, D. S., M. E. Gälli, P. J. Silva, & K. A. Prather, 2000: Relative Sensitivity Factors for
915 Alkali Metal and Ammonium Cations in Single-Particle Aerosol Time-of-Flight
916 Mass Spectra. *Analytical Chemistry*, **72**(2), 416-422. doi: 10.1021/ac990434g
- 917 Han, C., Y. Liu, J. Ma, & H. He, 2012: Key role of organic carbon in the sunlight-enhanced
918 atmospheric aging of soot by O(2). *Proceedings of the National Academy of Sciences
919 of the United States of America*, **109**(52), 21250-21255. doi:
920 10.1073/pnas.1212690110
- 921 Hatch, L. E., K. A. Pratt, J. A. Huffman, J. L. Jimenez, & K. A. Prather, 2014: Impacts of
922 Aerosol Aging on Laser Desorption/Ionization in Single-Particle Mass
923 Spectrometers. *Aerosol Science and Technology*, **48**(10), 1050-1058. doi:
924 10.1080/02786826.2014.955907
- 925 Haynes, I., 1997: HASTELLOY® X ALLOY [Brochure]. Kokomo, IN: Author.
- 926 Healy, R. M., J. Sciare, L. Poulain, M. Crippa, A. Wiedensohler, A. S. H. Prévôt, et al., 2013:
927 Quantitative determination of carbonaceous particle mixing state in Paris using
928 single-particle mass spectrometer and aerosol mass spectrometer measurements.
929 *Atmos. Chem. Phys.*, **13**(18), 9479-9496. doi: 10.5194/acp-13-9479-2013
- 930 Hendricks, J., B. Kärcher, U. Lohmann, & M. Ponater, 2005: Do aircraft black carbon
931 emissions affect cirrus clouds on the global scale? *Geophysical Research Letters*,
932 **32**(12), n/a-n/a. doi: 10.1029/2005GL022740
- 933 Herndon, S. C., J. T. Jayne, P. Lobo, T. B. Onasch, G. Fleming, D. E. Hagen, et al., 2008:
934 Commercial Aircraft Engine Emissions Characterization of in-Use Aircraft at
935 Hartsfield-Jackson Atlanta International Airport. *Environmental Science &
936 Technology*, **42**, 1877-1883. doi: 10.1021/es072029+
- 937 ICAO, 2008: Annex 16 to the Convention on International Civil Aviation: Environmental
938 Protection: Volume II Aircraft Engine Emissions. (3rd).
- 939 ICAO, 2013: Environmental Report. Aviation and Climate Change.
- 940 IPCC, 1999: Aviation and the global atmosphere. A special report of Intergovernmental
941 Panel on Climate Change working groups I and III. In J. E. Penner, D. H. Lister, D.
942 J. Griggs, D. J. Dokken, & M. McFarland (Eds.). Cambridge, UK and New York,
943 NY, USA: Cambridge University Press, UK.
- 944 IPCC, 2007: Climate Change 2007 - The Physical Science Basis: Working Group I
945 Contribution to the Fourth Assessment Report of the Intergovernmental Panel on
946 Climate Change. In S. Solomon, D. Qin, M. Manning, Z. Chen, M. Marquis, K. B.
947 Averyt, M. Tignor, & H. L. Miller (Eds.): Cambridge University Press, UK.

- 948 Janssen, N. A., M. E. Gerlofs-Nijland, T. Lanki, R. O. Salonen, F. Cassee, G. Hoek, et al.
949 (2012). *Health effects of black carbon*. World Health Organization, Copenhagen.
- 950 Jeong, C. H., M. L. McGuire, K. J. Godri, J. G. Slowik, P. J. G. Rehbein, & G. J. Evans,
951 2011: Quantification of aerosol chemical composition using continuous single
952 particle measurements. *Atmos. Chem. Phys.*, *11*(14), 7027-7044. doi: 10.5194/acp-
953 11-7027-2011
- 954 Kärcher, B., O. Möhler, P. J. DeMott, S. Pechtl, & F. Yu, 2007: Insights into the role of soot
955 aerosols in cirrus cloud formation. *Atmos. Chem. Phys.*, *7*(16), 4203-4227. doi:
956 10.5194/acp-7-4203-2007
- 957 Kinsey, J. S., M. D. Hays, Y. Dong, D. C. Williams, & R. Logan, 2011: Chemical
958 Characterization of the Fine Particle Emissions from Commercial Aircraft Engines
959 during the Aircraft Particle Emissions eXperiment (APEX) 1 to 3. *Environmental
960 Science & Technology*, *45*(8), 3415-3421. doi: 10.1021/es103880d
- 961 Kolaitis, L. N., F. J. Bruynseels, R. E. Van Grieken, & M. O. Andreae, 1989: Determination
962 of methanesulfonic acid and non-sea-salt sulfate in single marine aerosol particles.
963 *Environmental Science & Technology*, *23*(2), 236-240. doi: 10.1021/es00179a018
- 964 Lee, D. S., D. W. Fahey, P. M. Forster, P. J. Newton, R. C. N. Wit, L. L. Lim, et al., 2009:
965 Aviation and global climate change in the 21st century. *Atmospheric Environment*,
966 *43*, 3520-3537. doi: 10.1016/j.atmosenv.2009.04.024
- 967 Liati, A., B. T. Brem, L. Durdina, M. Vöggtli, Y. Arroyo Rojas Dasilva, P. Dimopoulos
968 Eggenschwiler, et al., 2014: Electron Microscopic Study of Soot Particulate Matter
969 Emissions from Aircraft Turbine Engines. *Environmental Science & Technology*,
970 *48*(18), 10975-10983. doi: 10.1021/es501809b
- 971 Liu, D.-Y., K. A. Prather, & S. V. Hering, 2000: Variations in the Size and Chemical
972 Composition of Nitrate-Containing Particles in Riverside, CA. *Aerosol Science and
973 Technology*, *33*(1-2), 71-86. doi: 10.1080/027868200410859
- 974 Lobo, P., L. Durdina, G. J. Smallwood, T. Rindlisbacher, F. Siegerist, E. A. Black, et al.,
975 2015: Measurement of Aircraft Engine Non-Volatile PM Emissions: Results of the
976 Aviation - Particle Regulatory Instrument Demonstration Experiment (A-PRIDE) 4
977 Campaign. *Aerosol Science and Technology*, 00-00. doi:
978 10.1080/02786826.2015.1047012
- 979 Mauney, T., F. Adams, & M. R. Sine, 1984: Carbonaceous Particles in the Atmosphere 1983
980 Laser microprobe mass spectrometry of environmental soot particles. *Science of The
981 Total Environment*, *36*, 215-224. doi: [http://dx.doi.org/10.1016/0048-
982 9697\(84\)90269-9](http://dx.doi.org/10.1016/0048-9697(84)90269-9)
- 983 Mazaheri, M., T. E. Bostrom, G. R. Johnson, & L. Morawska, 2013: Composition and
984 Morphology of Particle Emissions from in-use Aircraft during Takeoff and Landing.
985 *Environmental Science & Technology*, *47*, 5235-5242. doi: 10.1021/es3046058
- 986 Miller, R. A., 1997: Thermal barrier coatings for aircraft engines: history and directions.
987 *Journal of Thermal Spray Technology*, *6*(1), 35-42. doi: 10.1007/BF02646310
- 988 Onasch, T. B., J. T. Jayne, S. Herndon, D. R. Worsnop, R. C. Mlake-Lye, I. P. Mortimer, et
989 al., 2009: Chemical Properties of Aircraft Engine Particulate Exhaust Emissions.
990 *Journal of Propulsion and Power*, *25*, 1121-1137. doi: 10.2514/1.36371
- 991 Pagan, I., D. L. Costa, J. K. McGee, J. H. Richards, J. A. Dye, & M. J. Dykstra, 2003: Metals
992 Mimic Airway Epithelial Injury Induced by in Vitro Exposure to Utah Valley

- 993 Ambient Particulate Matter Extracts. *Journal of Toxicology and Environmental*
 994 *Health, Part A*, 66(12), 1087-1112. doi: 10.1080/15287390390213908
- 995 Park, K., D. B. Kittelson, M. R. Zachariah, & P. H. McMurry, 2004: Measurement of
 996 Inherent Material Density of Nanoparticle Agglomerates. *Journal of Nanoparticle*
 997 *Research*, 6, 267-272. doi: 10.1023/B:NANO.0000034657.71309.e6
- 998 Pastor, S. H., J. O. Allen, L. S. Hughes, P. Bhave, G. R. Cass, & K. A. Prather, 2003:
 999 Ambient single particle analysis in Riverside, California by aerosol time-of-flight
 1000 mass spectrometry during the SCOS97-NARSTO. *Atmospheric Environment*, 37,
 1001 *Supplement 2*, 239-258. doi: [http://dx.doi.org/10.1016/S1352-2310\(03\)00393-5](http://dx.doi.org/10.1016/S1352-2310(03)00393-5)
- 1002 Petzold, A., & F. P. Schröder, 1998: Jet Engine Exhaust Aerosol Characterization. *Aerosol*
 1003 *Science and Technology*, 28(1), 62-76. doi: 10.1080/02786829808965512
- 1004 Qiu, C., A. F. Khalizov, B. Hogan, E. L. Petersen, & R. Zhang, 2014: High Sensitivity of
 1005 Diesel Soot Morphological and Optical Properties to Combustion Temperature in a
 1006 Shock Tube. *Environmental Science & Technology*, 48(11), 6444-6452. doi:
 1007 10.1021/es405589d
- 1008 Rogers, F., P. Arnott, B. Zielinska, J. Sagebiel, K. E. Kelly, D. Wagner, et al., 2005: Real-
 1009 Time Measurements of Jet Aircraft Engine Exhaust. *Journal of the Air & Waste*
 1010 *Management Association*, 55, 583-593. doi: 10.1080/10473289.2005.10464651
- 1011 Rudich, Y., N. M. Donahue, & T. F. Mentel, 2007: Aging of Organic Aerosol: Bridging the
 1012 Gap Between Laboratory and Field Studies. *Annual Review of Physical Chemistry*,
 1013 58, 321-352. doi: 10.1146/annurev.physchem.58.032806.104432
- 1014 Schumann, U., 1996: On Conditions for Contrail Formation from Aircraft Exhausts.
 1015 *Meteorologische Zeitschrift / DLR, Inst. f. Physik der Atmosphäre, Report No. 44*, 5,
 1016 4-23.
- 1017 Shapiro, M., P. Vainshtein, D. Dutcher, M. Emery, M. Stolzenburg, D. B. Kittelson, et al.,
 1018 2012: Characterization of agglomerates by simultaneous measurement of mobility,
 1019 vacuum aerodynamic diameter and mass. *Journal of Aerosol Science*, 44, 24-45. doi:
 1020 10.1016/j.jaerosci.2011.08.004
- 1021 Silva, P. J., R. A. Carlin, & K. A. Prather, 2000: Single particle analysis of suspended soil
 1022 dust from Southern California. *Atmospheric Environment*, 34(11), 1811-1820. doi:
 1023 [http://dx.doi.org/10.1016/S1352-2310\(99\)00338-6](http://dx.doi.org/10.1016/S1352-2310(99)00338-6)
- 1024 Silva, P. J., & K. A. Prather, 2000: Interpretation of Mass Spectra from Organic Compounds
 1025 in Aerosol Time-of-Flight Mass Spectrometry. *Analytical Chemistry*, 72(15), 3553-
 1026 3562. doi: 10.1021/ac9910132
- 1027 Spencer, M. T., & K. A. Prather, 2006: Using ATOFMS to Determine OC/EC Mass
 1028 Fractions in Particles. *Aerosol Science and Technology*, 40, 585-594. doi:
 1029 10.1080/02786820600729138
- 1030 Terzano, C., F. Di Stefano, V. Conti, E. Graziani, & A. Petroianni, 2010: Air pollution
 1031 ultrafine particles: toxicity beyond the lung. *Eur Rev Med Pharmacol Sci*, 14(10),
 1032 809-821.
- 1033 Timko, M. T., T. B. Onasch, M. J. Northway, J. T. Jayne, M. R. Canagaratna, S. C. Herndon,
 1034 et al., 2010: Gas Turbine Engine Emissions—Part II: Chemical Properties of
 1035 Particulate Matter. *Journal of Engineering for Gas Turbines and Power*, 132(6),
 1036 061505-061505. doi: 10.1115/1.4000132

- 1037 Touri, L., H. Marchetti, I. Sari-Minodier, N. Molinari, & P. Chanez, 2013: The airport
1038 atmospheric environment: respiratory health at work. *European Respiratory Review*,
1039 **22**(128), 124-130. doi: 10.1183/09059180.00005712
- 1040 TSI, I., 2004: Series 3800 Aerosol Time-of-Flight Mass Spectrometers with Aerodynamic
1041 Focusing Lens Technology. Shoreview, MN.
- 1042 Yim, S. H. L., G. L. Lee, I. H. Lee, F. Allroggen, A. Ashok, F. Caiazzo, et al., 2015: Global,
1043 regional and local health impacts of civil aviation emissions. *Environmental*
1044 *Research Letters*, **10**, 034001. doi: 10.1088/1748-9326/10/3/034001
- 1045 Zhou, C., & J. E. Penner, 2014: Aircraft soot indirect effect on large-scale cirrus clouds: Is
1046 the indirect forcing by aircraft soot positive or negative? *Journal of Geophysical*
1047 *Research: Atmospheres*, **119**(19), 11,303-311,320. doi: 10.1002/2014JD021914
- 1048